# Calibrating the Cryogenian

Francis A. Macdonald,[1]* Mark D. Schmitz,[2] James L. Crowley,[2] Charles F. Roots,[3] David S. Jones,[4] Adam C. Maloof,[5] Justin V. Strauss,[6] Phoebe A. Cohen,[1] David T. Johnston,[1] Daniel P. Schrag[1]

The Neoproterozoic was an era of great environmental and biological change, but a paucity of direct and precise age constraints on strata from this time has prevented the complete integration of these records. We present four high-precision U-Pb ages for Neoproterozoic rocks in northwestern Canada that constrain large perturbations in the carbon cycle, a major diversification and depletion in the microfossil record, and the onset of the Sturtian glaciation. A volcanic tuff interbedded with Sturtian glacial deposits, dated at 716.5 million years ago, is synchronous with the age of the Franklin large igneous province and paleomagnetic poles that pin Laurentia to an equatorial position. Ice was therefore grounded below sea level at very low paleolatitudes, which implies that the Sturtian glaciation was global in extent.

Middle Neoproterozoic or Cryogenian strata [850 to 635 million years ago (Ma)] contain evidence for the breakup of the supercontinent Rodinia, widespread glaciation (1, 2), high-amplitude fluctuations in geochemical proxy records (3), and the radiation of early eukaryotes (4); however, both relative and absolute age uncertainties have precluded a

[1]Department of Earth and Planetary Sciences, Harvard University, Cambridge, MA 02138, USA. [2]Department of Geosciences, Boise State University, Boise, ID 83725, USA. [3]Geological Survey of Canada, Whitehorse, YT YIA 1B5, Canada. [4]Department of Earth and Planetary Sciences, Washington University, St. Louis, MO 63130, USA. [5]Department of Geosciences, Princeton University, Princeton, NJ 08544, USA. [6]555 East Simpson Street, Jackson, WY 83001, USA.

*To whom correspondence should be addressed. E-mail: fmacdon@fas.harvard.edu

better understanding of the nature and interrelationships of these events. Several first-order questions remain: How many Neoproterozoic glaciations were there? How were they triggered? What was their duration and extent? How did the biosphere respond? Answers to all of these questions hinge on our ability to precisely correlate and calibrate data from disparate stratigraphic records around the world.

The snowball Earth hypothesis (1, 2) was developed in response to strong paleomagnetic evidence for low-latitude glaciation from the Elatina Formation in Australia (5, 6). The Elatina Formation and its distinct cap carbonate have been correlated with chemo- and lithostratigraphy to Marinoan-age glacial deposits in the Ghaub Formation in Namibia (635.5 ± 0.6 Ma) (7); the Nantuo Formation in South China

(636.3 ± 4.9 Ma) (8), which underlies the cap carbonate of the basal Doushantuo Formation (635.2 ± 0.2 Ma) (9); and other glacial deposits around the globe, including the Ice Brook Formation in northwestern Canada (10). In contrast, a paucity of robust paleomagnetic poles and precise age constraints from volcanic rocks directly interbedded with early Cryogenian glacial deposits has precluded tests of the snowball Earth hypothesis for the Sturtian glaciation. The global nature of the Sturtian glaciation has been inferred from the ubiquitous occurrence of glacial deposits that are stratigraphically below Marinoan diamictite units (10) as well as banded iron formation within these deposits (1).

We present four high-precision U-Pb isotope dilution–thermal ionization mass spectrometry (ID-TIMS) dates from intrusive and volcanic rocks within Neoproterozoic strata of northwestern Canada. These dates, coupled with high-resolution $\delta^{13}C$ profiles (11), allow us to synthesize Cryogenian geological, geochemical, paleomagnetic, and paleontological data both regionally and globally. The accurate integration of these records places hard constraints on the timing and extent of the Sturtian glaciation and its relationship to the Franklin large igneous province (LIP) and the Cryogenian microfossil record.

Neoproterozoic strata are exposed in erosional windows (inliers) through Paleozoic carbonate rocks in northwestern Canada for more than 1500 km, from the Alaska border
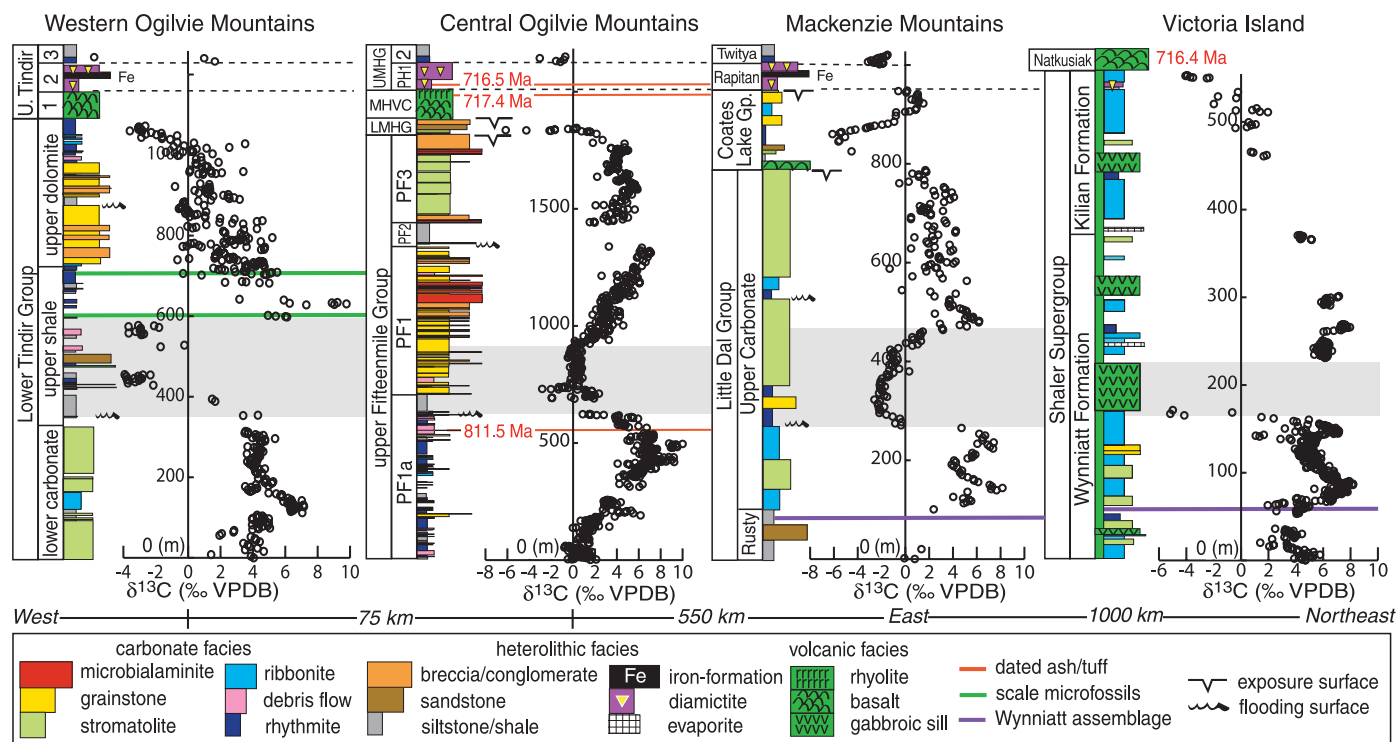
**Fig. 1.** Composite chemo- and lithostratigraphy of Neoproterozoic strata in northwestern Canada, including the Upper and Lower Tindir Groups (13), the Fifteenmile and Lower Mount Harper Group (table S2), the Little Dal Group (3), the Coates Lake Group (table S2), the Twitya Formation (3), and the Shaler Supergroup (18). Shaded area represents the Bitter Springs isotopic stage (3).

east through the Ogilvie and Wernecke Mountains of Yukon, to the Mackenzie Mountains of the Northwest Territories, and north to Victoria Island of Nunavut (fig. S1A). Exposures in the Coal Creek inlier of the central Ogilvie Mountains consist of mixed carbonate and siliciclastic rocks of the upper Fifteenmile and Lower Mount Harper Groups (LMHG), bimodal volcanic rocks of the Mount Harper volcanic complex (MHVC) (12), and glacial diamictite of the Upper Mount Harper Group (UMHG) (Fig. 1). A glacial origin for the UMHG is inferred from bed-penetrating dropstones with impact margins and outsized clasts in fine, laminated beds, and by striated clasts in exposures in the Hart River inlier of the eastern Ogilvie Mountains (fig. S2). Evidence for grounded ice is provided by glacial push structures and soft-sedimentary deformation (fig. S2). The UMHG and the iron-rich unit 2 of the Upper Tindir Group in the western Ogilvie Mountains are correlative with the Sturtian-age Sayunei Formation of the Rapitan Group in the Mackenzie Mountains (13, 14). The broad distribution of massive diamictite and stratified glacial deposits with coarse-grained ice-rafted debris in the Rapitan Group of the Northwest Territories (14, 15) and its correlatives in Yukon and Alaska (fig. S3) suggests the proximity to a marine ice grounding line.

The MHVC previously was dated with multigrain U-Pb ID-TIMS analyses at $751^{+26}_{-18}$ Ma (16). We collected a quartz-phyric rhyolite of member D from the same site (fig. S1) that yielded a weighted mean $^{206}Pb$-$^{238}U$ zircon date of 717.43 ± 0.14 Ma, interpreted as the eruptive age of this unit (fig. S4). This ~33-million-year age revision is likely due to inherited cores in the previously dated multigrain zircon fractions, resulting in an artificially old age. Below the MHVC, a green, flinty, bedded tuff within allodapic dolostone beds near the top of unit PF1a of the Fifteenmile Group yielded a weighted mean $^{206}Pb$-$^{238}U$ zircon date of 811.51 ± 0.25 Ma, interpreted as the time of deposition (fig. S4). Above the MHVC, a green to pink brecciated tuff within glacial deposits of the UMHG yielded a weighted mean $^{206}Pb$-$^{238}U$ zircon date of 716.47 ± 0.24 Ma, interpreted as the deposition age (fig. S4).

In the Minto inlier on Victoria Island (fig. S1), zircon and baddeleyite from gabbroic sills and dikes from the Franklin LIP previously were dated at $723^{+4}_{-2}$ Ma and 718 ± 2 Ma (17). Our Franklin LIP sample is from a coarse-grained diabase sill, >20 m thick, intruding the middle of the Wynniatt Formation (18), which yielded a weighted mean $^{206}Pb$-$^{238}U$ baddeleyite date of 716.33 ± 0.54 Ma (fig. S4). We interpret the apparent discrepancy between our result and previous ages (17) as an artifact of comparing upper intercept and $^{207}Pb$/$^{206}Pb$ dates with our $^{206}Pb$/$^{238}U$ dates in light of recently recognized systematic error in the U decay constant ratio (11, 19).

This geochronology reveals the >3000-km extent of the Franklin LIP (~716.5 Ma), from the Yukon-Alaska border to Ellesmere Island, where mafic dikes have been dated at 716 ± 1 Ma (20). Although no evidence for prevolcanic extension and rifting is present on Victoria Island (21), conspicuous normal faulting exists within the LMHG and the lower suite of the MHVC (12), temporally linking the Franklin LIP to extension on the northwestern Laurentian margin.

Several paleomagnetic studies on strongly magnetized mafic dikes, sills, and lavas have demonstrated that the Franklin LIP was emplaced when northwestern Laurentia was within 10° of the equator (6, 22, 23). The dated sill and the sediments that it intrudes on Victoria Island yield paleomagnetic data that are consistent with the previous low-latitude results (18). The age of the tuff interbedded with glacial deposits of the UMHC, 716.47 ± 0.24 Ma, is indistinguishable from the date of the Franklin LIP, 716.33 ± 0.54 Ma. Therefore, grounded ice was present on the northwestern margin of Laurentia at ~716.5 Ma, when it was situated at equatorial latitudes. Climate models have long predicted that if the ice line advanced equatorward of ~30° to 40°, an ice-albedo feedback would drive global glaciation (24, 25). Thus, we conclude that the Sturtian glaciation at ~716.5 Ma was global in nature.

It is uncertain whether the Sturtian glacial epoch consisted of one discrete glaciation that lasted tens of millions of years, or multiple glacial episodes including the low-latitude glaciation at ~716.5 Ma. Prior to this study, minimum and maximum age constraints on the Sturtian glaciation were provided by a sample from South China dated at 662.9 ± 4.3 Ma (26) and the Leger Granite in Oman dated at 726 ± 1 Ma (27), respectively. We suggest that our age from member D of the MHVC, 717.43 ± 0.14 Ma, provides a maximum age constraint on the low-latitude Sturtian glaciation not only because glacial deposits have not been identified below member D, but also because models suggest extremely rapid ice advance once ice is below 30° latitude (24, 25), such that glaciation of equatorial latitudes should be synchronous around the globe. Evidence for a pre-Sturtian glaciation at ~750 Ma (referred to as the Kaigas glaciation) was reported in southern Namibia (28), Zambia (29), and northwestern China (30). However, at these localities the contact relationship of the purported glacial deposit with the dated unit and the glacial origin of the deposit are sus-

**Fig. 2.** Neoproterozoic composite carbonate $\delta^{13}C$ chemostratigraphy with U-Pb ID-TIMS ages that are directly linked to isotopic profiles (11). Bars indicate the time spans of fossil assemblages representing eukaryotic crown groups. Asterisks indicate fossil groups of uncertain taxonomic affinity. Bars faded upward reflect uncertainty in the minimum age constraint; bars faded downward reflect uncertainty in the maximum age constraint. Dashes represent the time span where a fossil record has not been identified but for which the eukaryotic group's presence is inferred from its occurrence in Ediacaran or Phanerozoic strata. Dashes with question marks indicate that earlier records have been proposed but the relationships between these fossils and the crown groups are uncertain.
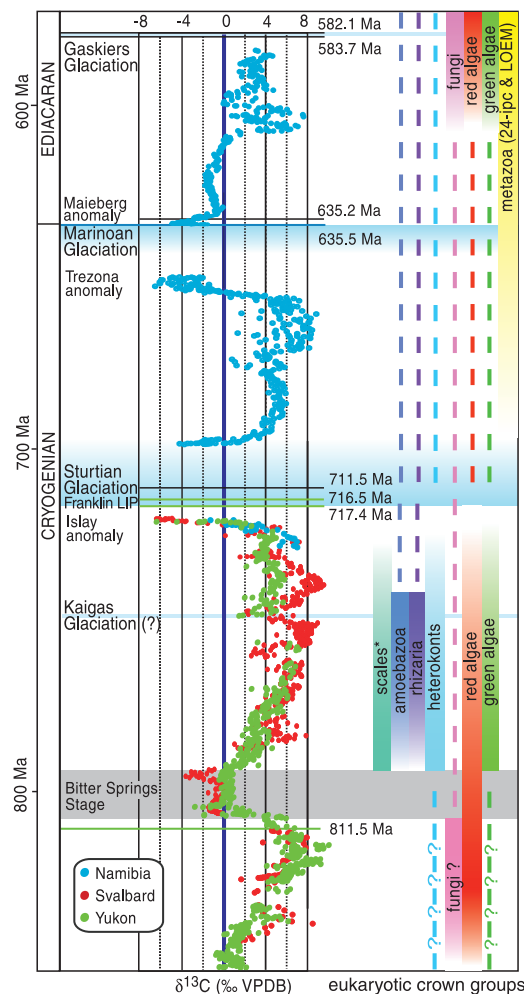
pect (*10*). Moreover, because there are no robust paleolatitude constraints on these rocks, the Kaigas glaciation may have been regional in extent. Previous Sturtian synglacial constraints at ~685 Ma were reported from Idaho (*31, 32*). However, these results have been questioned because the glacial nature of these deposits is uncertain, contacts between dated volcanic rocks and diamictites are tectonic, and repeated analyses have given different results (*10*). A $^{206}$Pb-$^{238}$U ID-TIMS date of 711.52 ± 0.20 Ma was reported from volcaniclastic rocks interbedded with glacigenic deposits within the Ghubrah Formation in Oman (*27*). Thus, if the Ghubrah Formation is recording the same glacial episode as the UMHG, the Sturtian glaciation lasted a minimum of 5 million years.

Using a recalibrated and expanded $\delta^{13}$C record, we can place the record of eukaryotic evolution in the context of geochemical perturbations and global glaciation (Fig. 2). The tuff dated at 811.5 Ma provides a maximum constraint on the Bitter Springs isotopic stage (*3*) and a useful benchmark for the calibration of early Neoproterozoic microfossil record. For instance, the chemostratigraphic position of the mineralized scale microfossils in the Lower Tindir Group of the western Ogilvie Mountains is above the Bitter Springs isotopic stage and below glacial deposits with banded iron formation that were previously correlated with the Rapitan Group (*13*). The Tindir microfossils are thus broadly coeval with complex microbiota described from the Chuar Formation in the Grand Canyon (older than 742 ± 6 Ma), the preglacial Beck Spring Formation of Death Valley, and the Svanbergfjellet Formation of Spitsbergen (*11*). Collectively, the calibration of these diverse microfossil records indicates that between the onset of the Bitter Springs isotopic stage (~811.5 Ma) and the Sturtian glaciation (~716.5 Ma), many major eukaryotic crown groups—members of Rhizaria, Amoebozoa, green and red algae, and vaucheriacean algae—had diverged and diversified. In contrast, the microfossil record between the Sturtian glaciation and the Marinoan glaciation (i.e., between ~716.5 and ~635 Ma) is depauperate; only simple acritarchs of unknown phylogenic affinity have been described (*4, 11*). This apparent bottleneck might be due in part to poor preservation and limited sampling, and/or the survival of some groups as cryptic forms. It is clear that a diverse biosphere persisted through the Neoproterozoic glaciations (*4*), but the impact of global glaciation on eukaryotic evolution remains unresolved.

With high-precision ages directly tied to the stratigraphic record we can begin to address the mechanisms behind Neoproterozoic environmental change. The presence of the Islay $\delta^{13}$C anomaly in the pre-Sturtian LMHG suggests a relationship between global carbon cycling and climate degradation (Figs. 1 and 2). Moreover, the synchrony among continental extension, the

Franklin LIP, and the Sturtian glaciation is consistent with the hypothesis that the drawdown of $CO_2$ via rifting and weathering of the low-latitude Franklin basalts could have produced a climate state that was more susceptible to glaciation (*25, 33*). However, even with the updated age constraints, it is unclear whether the bulk of the magmatism preceded or occurred during the glaciation.

### References and Notes

1. J. L. Kirschvink, in *The Proterozoic Biosphere*, J. W. Schopf, C. Klein, Eds. (Cambridge Univ. Press, Cambridge, 1992), pp. 51–52.
2. P. F. Hoffman, A. J. Kaufman, G. P. Halverson, D. P. Schrag, *Science* **281**, 1342 (1998).
3. G. P. Halverson, in *Neoproterozoic Geobiology and Paleobiology*, S. Xiao, A. J. Kaufman, Eds. (Springer, New York, 2006), pp. 231–271.
4. A. H. Knoll, E. J. Javaux, D. Hewitt, P. A. Cohen, *Philos. Trans. R. Soc. Lond. Sec. B Biol. Sci.* **361**, 1023 (2006).
5. L. E. Sohl, N. Christie-Blick, D. V. Kent, *Geol. Soc. Am. Bull.* **111**, 1120 (1999).
6. D. A. D. Evans, *Am. J. Sci.* **300**, 347 (2000).
7. K. H. Hoffmann, D. J. Condon, S. A. Bowring, J. L. Crowley, *Geology* **32**, 817 (2004).
8. S. Zhang, G. Jiang, Y. Han, *Terra Nova* **20**, 289 (2008).
9. D. J. Condon et al., *Science* **308**, 95 (2005).
10. P. F. Hoffman, Z.-X. Li, *Palaeogeogr. Palaeoclimatol. Palaeoecol.* **277**, 158 (2009).
11. See supporting material on *Science* Online.
12. P. S. Mustard, C. F. Roots, *Geol. Surv. Canada Bull.* **492** (1997).
13. F. A. Macdonald, P. A. Cohen, F. O. Dudás, D. P. Schrag, *Geology* **38**, 143 (2010).
14. G. M. Yeo, *Geol. Surv. Canada Pap. 81-10*, 25 (1981).
15. G. H. Eisbacher, *Geol. Surv. Canada Pap. 77-35* (1978), p. 1.
16. C. F. Roots, R. R. Parrish, *Geol. Surv. Canada Pap. 88-2* (1988), p. 29.
17. L. M. Heaman, A. N. LeCheminant, R. H. Rainbird, *Earth Planet. Sci. Lett.* **109**, 117 (1992).
18. D. S. Jones, thesis, Harvard University (2009).
19. B. Schoene, J. C. Crowley, D. J. Condon, M. D. Schmitz, S. A. Bowring, *Geochim. Cosmochim. Acta* **70**, 426 (2006).
20. S. W. Denyszyn, D. W. Davis, H. C. Halls, *Can. J. Earth Sci.* **46**, 155 (2009).
21. R. H. Rainbird, *J. Geol.* **101**, 305 (1993).
22. J. K. Park, *Precambrian Res.* **69**, 95 (1994).
23. H. C. Palmer, W. R. A. Baragar, M. Fortier, J. H. Foster, *Can. J. Earth Sci.* **20**, 1456 (1983).
24. G. R. North, R. F. Cahalan, J. A. Coakley Jr., *Rev. Geophys. Space Phys.* **19**, 91 (1981).
25. J. Bendtsen, *Clim. Dyn.* **18**, 595 (2002).
26. C. Zhou et al., *Geology* **32**, 437 (2004).
27. S. A. Bowring et al., *Am. J. Sci.* **307**, 1097 (2007).
28. H. E. Frimmel, U. S. Klotzli, P. R. Siegfried, *J. Geol.* **104**, 459 (1996).
29. R. M. Key et al., *J. Afr. Earth Sci.* **33**, 503 (2001).
30. B. Xu et al., *Precambrian Res.* **168**, 247 (2009).
31. K. Lund, J. N. Aleinikoff, K. V. Evans, C. M. Fanning, *Geol. Soc. Am. Bull.* **115**, 349 (2003).
32. C. M. Fanning, P. K. Link, *Geology* **32**, 881 (2004).
33. Y. Donnadieu, Y. Goddéris, G. Ramstein, A. Nédélec, J. Meert, *Nature* **428**, 303 (2004).
34. We thank the Yukon Geological Survey for assistance with logistics and helicopter support, T. Petach and S. Petersen for assistance in the field, and D. Pearce and H. Yntema for preparing samples. Supported by the Polar Continental Shelf Project and NSF Geobiology and Environmental Geochemistry Program grant EAR 0417422.

# The Role of Sulfuric Acid in Atmospheric Nucleation

Mikko Sipilä,[1,2,3]* Torsten Berndt,[1] Tuukka Petäjä,[2] David Brus,[4,5] Joonas Vanhanen,[2] Frank Stratmann,[1] Johanna Patokoski,[2] Roy L. Mauldin III,[6] Antti-Pekka Hyvärinen,[5] Heikki Lihavainen,[5] Markku Kulmala[2,7]

Nucleation is a fundamental step in atmospheric new-particle formation. However, laboratory experiments on nucleation have systematically failed to demonstrate sulfuric acid particle formation rates as high as those necessary to account for ambient atmospheric concentrations, and the role of sulfuric acid in atmospheric nucleation has remained a mystery. Here, we report measurements of new particles (with diameters of approximately 1.5 nanometers) observed immediately after their formation at atmospherically relevant sulfuric acid concentrations. Furthermore, we show that correlations between measured nucleation rates and sulfuric acid concentrations suggest that freshly formed particles contain one to two sulfuric acid molecules, a number consistent with assumptions that are based on atmospheric observations. Incorporation of these findings into global models should improve the understanding of the impact of secondary particle formation on climate.

Nucleation of particles in the atmosphere has been observed to be strongly dependent on the abundance of sulfuric acid ($H_2SO_4$) (*1–4*). Sulfur dioxide ($SO_2$), the precursor of $H_2SO_4$, has both natural and anthropogenic sources. Anthropogenic $SO_2$ emissions can have large indirect effects on climate if $H_2SO_4$ is responsible for atmospheric nucleation, but laboratory experiments have systematically failed to reproduce ambient new-particle formation rates as well as the nucleation rate dependence on the $H_2SO_4$ concentration (Table 1) (*5–15*).

Supporting Online Material for

**Calibrating the Cryogenian**

Francis A. Macdonald,* Mark D. Schmitz, James L. Crowley, Charles F. Roots, David S. Jones, Adam C. Maloof, Justin V. Strauss, Phoebe A. Cohen, David T. Johnston, Daniel P. Schrag

*To whom correspondence should be addressed. E-mail: fmacdon@fas.harvard.edu

**This PDF file includes:**

Materials and Methods

Figs. S1 to S4

Tables S1 and S2

References

<u>**Supporting Online Material**</u>

**Stratigraphic methods and results**

The upper Fifteenmile Group (*S1*) was measured along the ridgeline due north of Mount Harper (Fig. S1). Map unit PF1a (previously assigned to PR4 and PR5 in *S1*) consists of ~700 m of carbonate rocks and shale. The carbonate strata are composed predominately of rhythmite and ribbonite (i.e., dolosiltite deposited above storm wave base), with stromatolite bioherms present along strike. Dark colored, organic-rich limestone in unit PF1a commonly host molar tooth structures. The ca. 811.5 Ma age is from a 0.5 m thick bed of silicified, apple green tuff within limestone rhythmite beds, 541.5 m above the base of the measured section. Above the tuff are an additional 83 m of carbonate breccia and 73 m of black shale with stromatolite patch reefs. Map unit PF1a is succeeded by unit PF1, which is comprised of >600 m of dolomite grainstone shoals and microbialaminite with multiple exposure surfaces. Unit PF2 is a major transgressive sequence, consisting

of over 100 m of black shale. These facies shallow upwards to the distinct stromatolitic dolostone of unit PF3, which is correlative with the Callison Lake Dolostone in the Hart River Inlier (*S2*). Unit PF3 is 337 m thick and is overlain by the Lower Mount Harper Group (LMHG), which is exposed along the north side of the north-side-down Mount Harper Fault where it consists of up to 1.1 km of talus breccia, debris flow fanglomerate, and coalescing alluvial fans (*S3-S5*). Only the lower portion of the LMHG, consisting of dolomitic breccia and shale with lenticular dolomite beds, was measured for this study.

The Mount Harper volcanic complex (MHVC) is divided into 6 informal units that are defined both stratigraphically and compositionally (*S5, S6*). A lower suite, constituting members A-C, is of a basaltic chemical composition, and is composed of several hundreds of meters of pillow basalt, hyaloclastic breccia, and block and ash flows. The upper suite, which unconformably overlies members A-C, includes rhyolite of member D and andesite of members E and F. Member F andesites form pillowed flows, breccias, tuffs, and invasive flows that interfinger with and intrude into diamictite units of the Upper Mount Harper Group (UMHG). The *ca* 717.4 Ma age is from a quartz-phyric rhyolite of member D exposed at the top of a hill with no rocks present that are stratigraphically higher.

At Tango Tarn (F840, F917) and on the south flank of Mount Harper (F836; Figs. S1, S3), a maroon-coloured mudstone with pebble- to cobble- sized lonestones of dolomite and volcanic rocks forms the base of map unit PH1 of the UMHG. This rock closely resembles the Sayeuni Formation of the Rapitan Group in the Mackenzie Mountains (*S7*) and unit 2 of the Upper Tindir Group (*S8, S9*). The *ca* 716.5 Ma age is from an ~1 m thick, green to pink, brecciated tuff that rests above the maroon stratified

diamictite. We interpret this unit as a hyalo-tuff that formed in a subglacial eruption. The tuff interfingers with a massive diamictite unit that is >10 m thick and consists of dolomite and volcanic boulder clasts in a carbonate matrix. Above the massive diamictite is an additional ~10 m of fine-laminated, yellow weathering carbonate mudstone with bed-penetrating dropstones (Fig. S2). These dropstones display many characteristics of ice-rafted debris including impact margins and an association with many other small lonestones within the fine-laminated sediment. At Tango Tarn, the well-stratified diamictite beds are overlain by an additional >50 m of massive, weakly stratified diamictite. The diamictite units of unit PH1 display large lateral facies changes, and contain soft sedimentary deformation, suggesting the presence of grounded ice. In the Hart River inlier the soft sedimentary deformation rests directly under massive diamictite units that contain striated clasts (Fig. S2). Both the Rapitan Group and the diamictite of the UMHG are capped with dark-grey, flaggy limestone and shale, which host sharp negative $\delta^{13}$C anomalies (Fig. 1), characteristic of Sturtian-age cap carbonates globally (*S10*).

**Construction of the composite Cryogenian carbon isotope curve and paleontological record**

To minimize miscorrelations, we have used a minimum number of sections to construct our composite carbon isotope curve (Fig. 2). The curve is hung from the upper Fifteenmile Group as it is the only Cryogenian carbonate carbon-isotope curve with multiple U-Pb ID-TIMS age constraints directly tied to the stratigraphy. The upper Fifteenmile Group carbon-isotope data is stretched between the 811.5 Ma tuff in unit

PF1a, near the base of the Bitter Springs isotopic stage, and the 717.4 Ma rhyolite in the Mount Harper Group. We acknowledge that there may be a significant hiatus between units PF1 and PF2.

The age of the *Bangiomorpha* assemblage from the Hunting Formation in Arctic Canada, representing the red algae crown group (*S11*), is poorly constrained. The Hunting Formation overlies strata intruded by the 1267 ± 2 Ma Mackenzie dikes (*S12*) and is intruded by the 723-718 Ma Franklin magmatic suite (*S13*). An unpublished Pb-Pb age on carbonate from the presumably correlative Society Cliffs Formation on Baffin Island of 1198 ± 24 Ma has been previously used to support a ca. 1200 Ma age of the fossil assemblage (*S11*), but Pb can move freely in carbonate (*S14*), and thus this age cannot be relied upon. Carbon isotope values through the Hunting Formation range from +2 to +4‰, but lack any distinct features that permit a robust correlation (*S15*). In Figure 2 we use a faded bar to signify the age uncertainty for the Hunting Formation and the earliest evidence of red algae. As green algae are sister to red algae, the presence of crown group red algae as fossils also indicates the presence of total group green algae. Because there is a lack of direct fossil evidence for the presence of green algae before the Bitter Springs isotopic stage, we have placed a dashed line with question marks for green algae during this period.

The Wynniatt Formation of arctic Canada is one of the most fossiliferous units in the Proterozoic (*S16-S18*). Diverse and abundant well-preserved organic walled microfossils have been described from narrow horizons of black shale from near the top of member 2 of the Wynniatt Formation. The fossil biota includes numerous morphologically complex eukaryotes, including multicellular taxa. However, the

taxonomic affinities of most of these fossils, including *Tappania plana* and *Cheilofilum hysteriopsis,* remain enigmatic. Fungal affinities for both are possible, though not enough morphological characters exist for a definitive taxonomic assignment (*S19*). A similar, though less diverse assemblage, occurs in the Rusty Shale Formation of the Little Dal Group in the Mackenzie Mountains (*S16*). Carbon and strontium isotope analyses indicate that the lower Wynniatt Formation is correlative with the Rusty Shale Formation and that both were deposited prior to the Bitter Springs isotopic stage (*S20*). Despite the difficulties in placing these taxa within known crown groups, their morphologies indicate that by *ca* 811.5 Ma, eukaryotic organisms had evolved capabilities for cell differentiation, three-dimensional organization, and complex cytoskeletal architecture (*S19*).

The upper portion of the Lower Tindir Group of the western Ogilvie Mountains contain mineralized scale microfossils, and is correlated with PF1 of the upper Fifteenmile Group and the positive peak above the Bitter Springs stage (*S8*). This correlation is supported by Sr isotopes in strata bracketing the scale microfossils that give values between 0.7065 and 0.7068, which are typical for this interval (*S8*). The scale microfossils in the Lower Tindir Group likely represent the oldest known evidence of eukaryotic biomineralization, but their taxonomic affinity is uncertain (asterisk in Fig. 2) (*S8*). The 'scales' bar is faded upwards because it is unclear exactly when during this pre-Sturtian interval deposition of the Lower Tindir Group terminates.

The carbon isotope and paleontological record of the Akademikerbreen Group in Svalbard is split into three segments: a pre-G1 segment, a Bitter Springs segment, and a post S1 segment (*S21*). These segments are then stretched to fit the upper Fifteenmile

Group. *Palaeovaucheria* and *Proterocladus*, representing the crown groups of chromalveolates and green algae, respectively, have been described in the upper portion of the Svanbergfjellet Formation, which spans time above the S1 surface and the Bitter Springs isotopic stage (*S19, S22, S23*). Consequently we have faded the bars for chromalveolates and green algae upwards from the Bitter Springs isotopic stage. We have included a dash with question marks below the chromalveolates bar down to represent the possibility that the >1 Ga *Palaovaucheria* from Siberia is a xanthophyte (*S19*).

Members of the rhizarian and amoebazoan crown groups are represented in the pre-742 Ma Chuar Group (*S24, S25*). The 742 ± 6 Ma age is from an ash in the upper-most portion of the Chuar Group and provides a time horizon from which to hang the Chuar paleontological record. A *ca* 770 Ma age on authigenic monazite has been previously cited as a maximum age of the Chuar Group (*S26*), however, this monazite is secondary, and is strictly a minimum age. If the Chuar Group was deposited in a rift graben, relatively fast depositional rates could be inferred (*S27*), but this conclusion is not supported by the stratigraphy, which is notably lacking in coarse detritus and other typical rift related lithologies (*S26*). Thus, it is unclear when deposition of the Chuar Group began, and we have faded the bars for rhizarian and amoebazoan down from the 742 Ma age. It is unlikely that vase shaped microfossils in the Chuar Group occur prior to the Bitter Springs stage as they are in the Kwagunt Formation, which forms the uppermost portion of the Chuar Group. Because carbonate carbon isotopes are rare in the Chuar group, stable isotopes are not helpful in refining this age (*S26*).

Microfossils described in the Sturtian-age Kingston Peak Formation of Death Valley (*S28, S29*) are in a structurally complicated area, in strata that has been mapped as

the underlying Beck Springs Formation (*S30*), and are quite similar to the fauna described in the Beck Springs Formation (*S31*). With this level of uncertainty we have excluded these forms from the inter-glacial portion of our composite.

The portion of the carbon isotope curve between the Sturtian and Marinoan glaciation begins at the 711.52 ± 0.20 Ma date on volcaniclastic rocks within the Gubrah Formation in Oman (*S32*). However, we acknowledge that the termination of the Sturtian glaciation could be as late as 662.9 ± 4.3 Ma (*S33*), and consequently we have faded the bar for the Sturtian glaciation upwards to reflect this uncertainty.

The late Cryogenian portion of the carbon isotope curve is provided from the pre-635 Ma Abeneb Group of Namibia (*S34, S35*). The lower diamictite in Namibia, the BIF bearing Chuos Formation, is correlated with the Rapitan Group and the Sturtian glaciation. The Cryogenian carbon isotope record from Mongolia is not included because the correlation between the Tayshir anomaly and the Trezona anomaly remains uncertain (*S36*). Because the ages of the termination of the Sturtian glaciation and the onset of the Marinoan glaciation are also uncertain, and there are no precise ages directly linked to this portion of the composite carbon isotope curve, it remains relatively loosely constrained.

The Marinoan glaciation has been dated at 635.5 ± 0.6 Ma (U-Pb ID-TIMS) in Namibia (*S35*). The carbon isotope record from the Ediacaran is provided by the post-635.5 Ma Tsumeb Subgroup of Namibia (*S34, S37*). The Ediacaran carbon isotope record of Mongolia is split at a major sequence boundary in the Tsagaan Oloom Formation (*36*). The demosponge biomarker 24-isopropylcholestane, representing the metazoan crown group, is present in and above the Fiq diamictite in Oman (*S38*), which contains ca. 645

Ma detrital zircons and has been correlated with the ca. 635 Ma Marinoan glaciation. The presence of metazoa in the early Ediacaran is further confirmed in the basal Doushantuo of South China with the presence of putative animal embryos within ornamented acritarchs (*S39*) as well as the Ediacaran acritarch record itself (*S40*). Members of the red and green algae crown groups are present in the phosphorites of the Doushantuo Formation at Weng'an (*S41*). The bars representing these finds are faded down to reflect the uncertainty in age in these deposits.

The carbon isotope curves from Namibia and Mongolia are stretched up to the ca. 582 Ma Gaskiers glaciation (*S42, S43*). It is inferred that the carbon isotope downturn and base-level fall recorded in these sections is in response to the glaciation, however there are no direct age constraints available that test this correlation.


**U-Pb ID-TIMS geochronology methods and results**

U-Pb dates were obtained from zircon and baddeleyite by the isotope dilution thermal ionization mass spectrometry (ID-TIMS) method. Zircon was subjected to a modified version of the chemical abrasion method of (*S44*), reflecting a preference to prepare and analyze carefully selected single crystals. Zircon separates were placed in a muffle furnace at 900°C for 60 hours in quartz beakers. Single annealed grains were selected and transferred to 3 ml Teflon PFA beakers with ultrapure $H_2O$ and then loaded into 300 µl Teflon PFA microcapsules. Fifteen microcapsules were placed in a large-capacity Parr vessel, and the crystals partially dissolved in 120 µl of 29 M HF for 10-12 hours at 180°C. The contents of each microcapsule were returned to 3 ml Teflon PFA beakers, the HF removed and the residual grains rinsed in ultrapure $H_2O$, immersed in 3.5 M $HNO_3$,

ultrasonically cleaned for an hour, and fluxed on a hotplate at 80°C for an hour. The HNO$_3$ was removed and the grains were rinsed several times with ultrapure H$_2$O before being reloaded into the same 300 μl Teflon PFA microcapsules (rinsed and fluxed in 6 M HCl during crystal sonication and washing) and spiked with the EARTHTIME mixed $^{233}$U-$^{235}$U-$^{205}$Pb tracer solution (ET535). The grains were dissolved in Parr vessels in 120 μl of 29 M HF with a trace of 3.5 M HNO$_3$ at 220°C for 48 hours, dried to salts, and then re-dissolved in 6 M HCl in Parr vessels at 180°C overnight. U and Pb were separated from the zircon matrix using an HCl-based anion-exchange chromatographic procedure (*S45*), eluted together and dried with 2 μl of 0.05 N H$_3$PO$_4$. Baddeleyite was treated in a similar manner to zircon, with the exceptions that it was not subjected to the annealing and chemical abrasion method, and it was fluxed in 3.5 M HNO$_3$ on a hotplate at 80°C for only 10 minutes prior to dissolution.

Pb and U were loaded on a single outgassed Re filament in 2 μl of a silica-gel/phosphoric acid mixture (*S46*), and U and Pb isotopic measurements made on a GVI (IsotopX) Isoprobe-T multicollector thermal ionization mass spectrometer equipped with an ion-counting Daly detector. Pb isotopes were measured by peak-jumping all isotopes on the Daly detector for 100 to 150 cycles, and corrected for $0.18 \pm 0.04\%$/a.m.u. (atomic mass unit) mass fractionation. Transitory isobaric interferences due to high-molecular weight organics, particularly on $^{204}$Pb and $^{207}$Pb, disappeared within approximately 30 cycles, while ionization efficiency averaged $10^4$ cps/pg of each Pb isotope. Linearity (to $\geq 1.4 \times 10^6$ cps) and the associated deadtime correction of the Daly detector were monitored by repeated analyses of NBS982, and have been constant since installation. Uranium was analyzed as UO$_2^+$ ions in static Faraday mode on $10^{11}$ ohm resistors for 150

to 200 cycles, and corrected for isobaric interference of $^{233}U^{18}O^{16}O$ on $^{235}U^{16}O^{16}O$ with an $^{18}O/^{16}O$ of 0.00206. Ionization efficiency averaged 20 mV/ng of each U isotope. U mass fractionation was corrected using the known $^{233}U/^{235}U$ ratio of the ET535 tracer solution.

U-Pb dates and uncertainties ($2\sigma$) were calculated using the algorithms of (*S47*), $^{235}U/^{205}Pb = 100.206$ and $^{233}U/^{235}U = 0.994746$ for the ET535 tracer solution (*S48*), and the U decay constants of (*S49*). $^{206}Pb/^{238}U$ ratios and dates were corrected for initial $^{230}Th$ disequilibrium using a Th/U$_{[magma]}$ of three, resulting in a systematic increase in the $^{206}Pb/^{238}U$ dates of ~90 kyr. All common Pb in analyses was attributed to laboratory blank and subtracted based on the measured laboratory Pb isotopic composition and associated uncertainty. U blanks were <0.1 pg, and small compared to sample amounts. Over the course of the experiment, analyses of the 500 Ma EARTHTIME standard solution yielded a weighted mean $^{206}Pb/^{238}U$ age of 499.85 ± 0.06 (n = 14, MSWD = 0.84), and a weighted mean $^{207}Pb/^{206}Pb$ age of 499.73 ± 0.42 (n = 14, MSWD = 1.4).

Ages of samples are interpreted from weighted means of equivalent $^{206}Pb/^{238}U$ dates. All data sets yield majority clusters of concordant (considering decay constant errors) and equivalent single zircon dates that we interpret as the igneous crystallization age of the zircons, and which approximate the eruption and deposition, or intrusive ages of the samples. We discard from age calculations the dates that are resolvably different than the majority cluster at the 95% confidence interval. Grains with older dates are interpreted as being xenocrysts and those with younger dates that are commonly discordant are interpreted as having suffered severe Pb loss not completely mitigated by chemical abrasion. Errors on individual analyses are based upon non-systematic

analytical uncertainties, including counting statistics, tracer subtraction, and blank Pb subtraction. Similarly non-systematic errors on the sample weighted mean ages are reported as internal 2σ, given the high probability of fit for all sample ages. These error estimates should be considered when comparing our $^{206}Pb/^{238}U$ dates with those from other laboratories that used the same EARTHTIME tracer solution or one that was cross-calibrated using EARTHTIME gravimetric standards. When comparing our dates with those derived from other decay schemes (e.g., $^{40}Ar/^{39}Ar$, $^{187}Re-^{187}Os$), the systematic uncertainties in tracer calibration and the $^{238}U$ decay constant should be added to the internal error in quadrature. This total systematic error ranges from ± 0.81 Ma for the youngest sample to ± 0.91 Ma for the oldest sample.

*Sample F834_147.5*

Four of eight dated zircons from F834_147.5 yielded concordant analyses with a weighted mean $^{206}Pb/^{238}U$ date of 811.51 ± 0.25 Ma (MSWD = 0.01), which is interpreted as the eruptive age (Fig. S4). Excluding one grain with an obvious inherited component, the rest of the analyses fall along a discordia array and are interpreted to have experienced variable amounts of recent Pb loss.

*Sample F837B*

Seven of ten dated zircons from F837B yielded concordant analyses with a weighted mean $^{206}Pb/^{238}U$ date of 717.43 ± 0.14 Ma (MSWD = 0.8), which is interpreted as the eruptive age (Fig. S4). Two slightly older grains were possibly inherited from the magma chamber, and the one younger grain likely experienced Pb loss. The ~33 million year age

revision from the previous date (*S50*) is most likely the result of inherited cores within the previous multigrain zircon analyses.

*Sample F840A*

Six of fourteen zircons dated from F840A form a majority cluster of concordant and equivalent analyses with a weighted mean $^{206}Pb/^{238}U$ ID-TIMS date of $716.47 \pm 0.24$ Ma (MSWD = 1.1)(Fig. S4), interpreted as the eruptive age of the tuff. Excluding one grain with an obvious inherited component, the rest of the analyses fall along a discordia array and are interpreted to have experienced variable amounts of recent Pb loss only partially mitigated by chemical abrasion. Longer chemical abrasion times (for fractions z21-z30) improved the recovery of concordant and equivalent ~716.5 Ma grains, supporting the interpretation of Pb loss in the younger grains. Nonetheless, we acknowledge the statistically less probable interpretation that a minor cluster of three grains with a weighted mean $^{206}Pb/^{238}U$ ID-TIMS date of $714.17 \pm 0.23$ Ma (Fig. S4) could represent the eruptive age if all ~716.5 Ma grains were inherited from the underlying volcanic complex.

*Sample S8*

Gabbroic sills and dikes on Victoria Island that are part of the Franklin LIP were previously dated at 723 +4/-2 Ma and 718 ± 2 Ma based on U-Pb upper intercept ages of discordant multi-grain fractions of zircon and baddeleyite (*S13*). We analyzed small (<100 ng) single baddeleyite crystals from sample S8. Five of seven grains yielded a weighted mean $^{206}Pb/^{238}U$ date of 716.33 ± 0.54 Ma (MSWD = 0.6), which is interpreted

as the emplacement age (Fig. S4). The two discordant grains fall on a discordia array, consistent with Pb loss. We interpret the apparent discrepancy of several million years between our result and previous ages (*S13*) as an artifact of comparing upper intercept (and $^{207}Pb/^{206}Pb$) dates from the previous study with our $^{206}Pb/^{238}U$ dates in light of recently recognized systematic error in the U decay constant ratio (*S51*). In fact, with one exception, the $^{206}Pb/^{238}U$ dates from (*S13*) are consistent with our more precise age estimate for Franklin LIP emplacement.

**Carbon and oxygen isotope methods**

During our mapping we collected samples at 1-4 m resolution for $\delta^{13}C$ and $\delta^{18}O$ analyses within measured stratigraphic sections. All samples were cut perpendicular to lamination, revealing internal textures. Between 5 and 20 mg of powder were micro-drilled from the individual laminations (where visible), avoiding veining, cleavage, and siliciclastic components. All subsequent isotopic analyses were performed on aliquots of this powder. Carbonate $\delta^{13}C$ and $\delta^{18}O$ isotopic data were acquired simultaneously on a VG Optima dual inlet mass spectrometer attached to a VG Isocarb preparation device (Micromass, Milford, MA) in the Harvard University Laboratory for Geochemical Oceanography. Approximately, 1-mg micro-drilled samples were reacted in a common, purified $H_3PO_4$ bath at 90°C. Evolved $CO_2$ was collected cryogenically and analyzed using an in-house reference gas. External error (1σ) from standards was better than ± 0.1‰ for both $\delta^{13}C$ and $\delta^{18}O$. Samples were calibrated to VPDB (Value of the Pee-Dee Belemnite) using the Cararra marble standard. Potential memory effect resulting from the common acid-bath system was minimized by increasing the reaction time for dolomite samples. Memory

effect is estimated at <0.1‰ based on variability of standards run after dolomite samples. Carbon ($\delta^{13}C$) and oxygen ($\delta^{18}O$) isotopic results are reported in per mil notation of $^{13}C/^{12}C$ and $^{18}O/^{16}O$, respectively, relative to the standard VPDB.
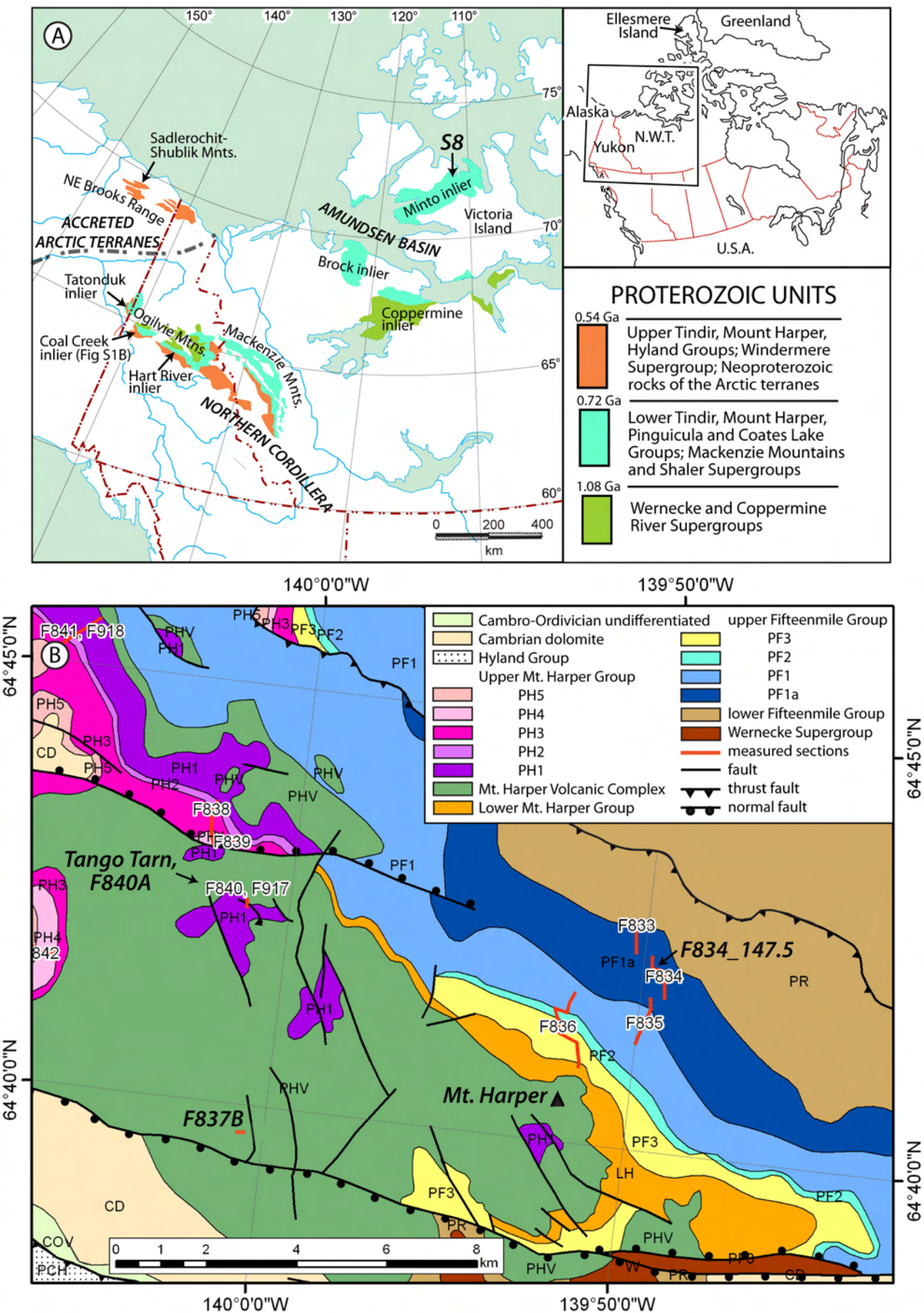
Figure S1: A) Location map of Proterozoic inliers in the northern Cordillera, modified from (S52). B) Geological map of the Mount Harper area, with locations of measured sections. Geological mapping by F.A. Macdonald and modified from (S1, S5).
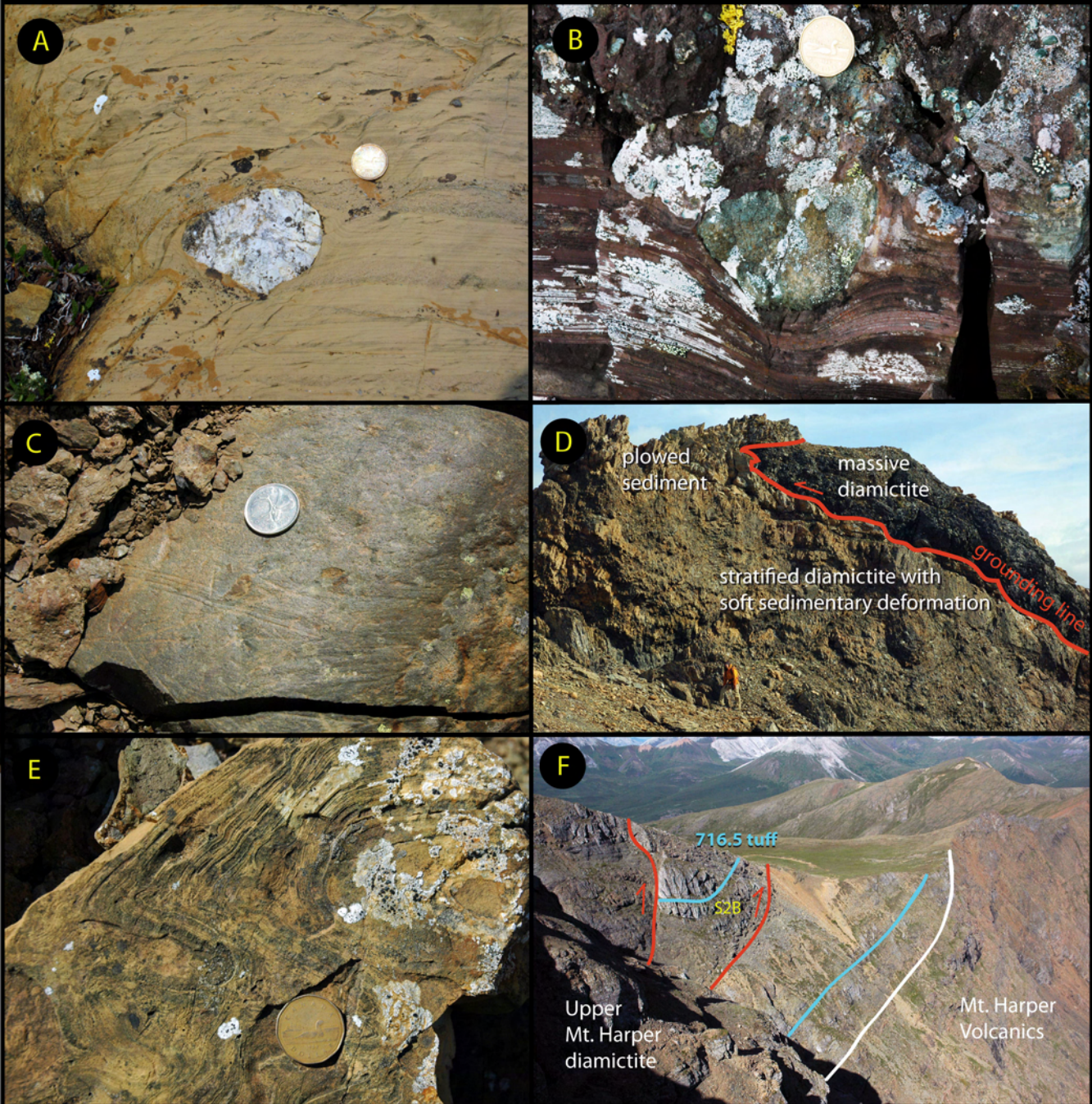
Figure S2: A) Glacial dropstone with impact margins from the Upper Mt. Harper Group (UMHG) in a unit above the 716.5 Ma tuff. The clast is composed of silicified dolomite from the underlying Fifteenmile Group. Canadian loonie for scale is 26.5 mm diameter. B) Bed-penetrating glacial dropstone in a maroon mudstone matrix from the UMHG below the 716.5 Ma tuff. Clast is composed of rhyolite from the Mt. Harper volcanic complex (MHVC). Canadian loonie for scale is 26.5 mm in diameter. See Fig. S2F for the location that the photo was taken. C) Striated clast from the UMHG in the Hart River inlier. Canadian quarter for scale is 23.8 mm in diameter. D) Glacial push structures with massive diamictite folding a yellow, dolomite matrix, stratified diamictite unit of the UMHG. View is southeastward with push-structures verging to the north. Hart River inlier at F936; geologist for scale. E) Soft sedimentary folds formed under grounded ice in the UMHG at Tango Tarn. Canadian loonie for scale is 26.5 mm in diameter. F) Exposure of 716.4 Ma tuff in the UMHG looking northwest, sections F840A and F917. Red lines are thrust faults with less than 20 m displacement, blue line is the dated volcanic horizon, and the white line is the contact between the MHVC and the UMHG. The yellow letters indicate the position of Fig. S2B. See Fig. S3 for a stratigraphic log of the section.
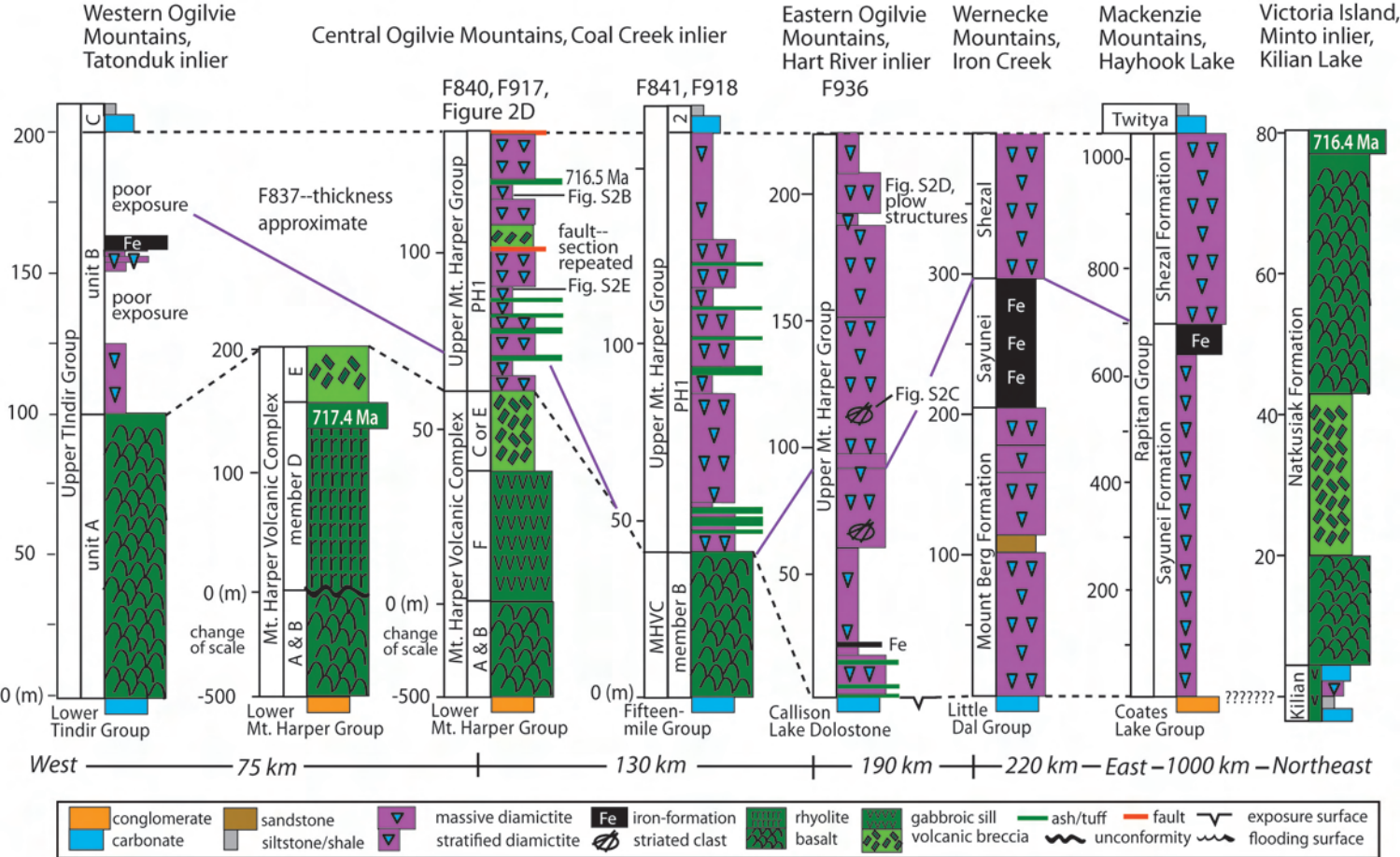
Figure S3: Measured sections of diamictite units in the Upper Tindir Group of the Tatonduk inlier from Macdonald et al. (S8), the Upper Mount Harper Group ~6 km west of Mount Harper (F837), Tango Tarn (F840, F917), ~6 km northwest of Tango Tarn (F841, F918), and in the Hart River inlier (F936), compared to those of the Rapitan Group in the Wernecke and Mackenzie Mountains (data courtesy of Paul Hoffman), and the Kilian and Natkusiak Formations of the Minto inlier. Purple line marks the top of the diamictite units with a maroon siltstone matrix, characteristic of the Sayunei Formation. Stratigraphic positions of diamictite facies photographed in Figure 2 are marked.

Figure S4: U-Pb Concordia diagrams for samples F834, F837B, F840A, and S8. Error ellipses are plotted at the 95% confidence interval; analyses accepted in the weighted mean calculations are shaded.

# Table S1. U-Pb isotopic data

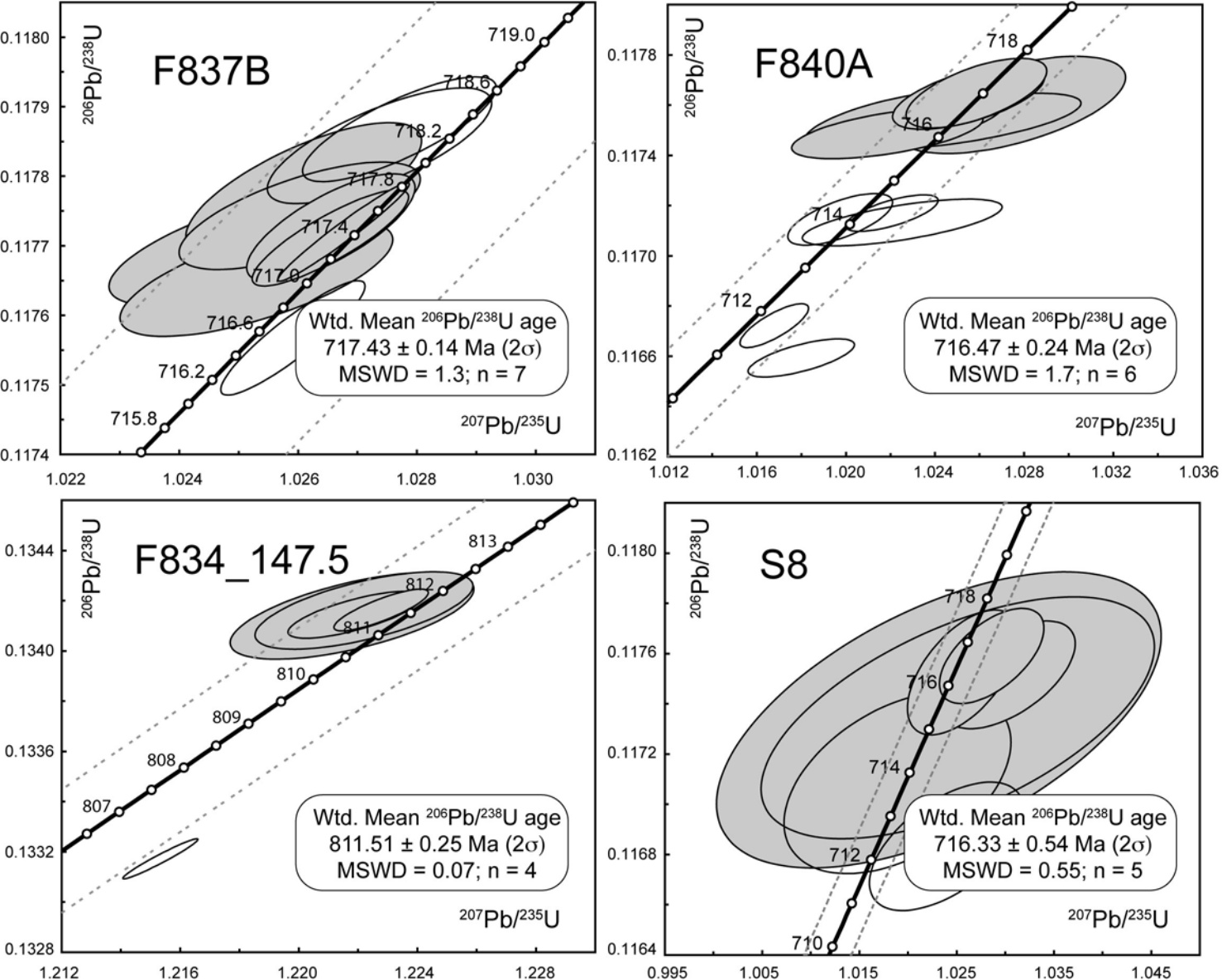| | | Compositional Parameters | | | | | | | | Radiogenic Isotope Ratios | | | | | | | | Isotopic Ages | | | | | |
|---|---|---|---|---|---|---|---|---|---|---|---|---|---|---|---|---|---|---|---|---|---|---|---|
| Sample | Wt. µg | U ppm | Th/U | Pb ppm | $^{206}Pb^*$ x10$^{-13}$ mol | mol % $^{206}Pb^*$ | Pb*/Pb$_c$ | Pb$_c$ (pg) | $^{206}Pb$/$^{204}Pb$ | $^{208}Pb$/$^{206}Pb$ | $^{207}Pb$/$^{206}Pb$ | % err | $^{207}Pb$/$^{235}U$ | % err | $^{206}Pb$/$^{238}U$ | % err | corr. coef. | $^{207}Pb$/$^{206}Pb$ | ± | $^{207}Pb$/$^{235}U$ | ± | $^{206}Pb$/$^{238}U$ | ± |
| (a) | (b) | (c) | (d) | (c) | (e) | (e) | (e) | (e) | (f) | (g) | (g) | (h) | (g) | (h) | (g) | (h) | (h) | (i) | (h) | (i) | (h) | (i) | (h) |
| **F837B** *(N64°39.757', W140°00.482')* | | | | | | | | | | | | | | | | | | | | | | | |
| z1 | 7.5 | 86 | 0.610 | 11.2 | 3.1613 | 99.25% | 42 | 1.95 | 2493 | 0.189 | 0.063174 | 0.160 | 1.025224 | 0.193 | 0.117702 | 0.058 | 0.681 | 714.08 | 3.4 | 716.54 | 0.99 | 717.32 | 0.39 |
| z2 | 7.7 | 204 | 0.348 | 24.3 | 7.7066 | 99.85% | 201 | 0.93 | 12733 | 0.108 | 0.063286 | 0.052 | 1.025916 | 0.097 | 0.117572 | 0.056 | 0.905 | 717.86 | 1.1 | 716.88 | 0.50 | 716.57 | 0.38 |
| z3 | 4.5 | 292 | 0.365 | 35.0 | 6.4441 | 99.82% | 159 | 0.98 | 10071 | 0.113 | 0.063241 | 0.082 | 1.026553 | 0.113 | 0.117728 | 0.053 | 0.741 | 716.35 | 1.7 | 717.20 | 0.58 | 717.47 | 0.36 |
| z4 | 4.0 | 111 | 0.617 | 14.5 | 2.1961 | 99.32% | 46 | 1.23 | 2748 | 0.191 | 0.063203 | 0.151 | 1.025294 | 0.184 | 0.117656 | 0.057 | 0.680 | 715.05 | 3.2 | 716.57 | 0.94 | 717.06 | 0.39 |
| z5 | 5.1 | 201 | 0.536 | 25.2 | 5.0615 | 99.75% | 124 | 1.03 | 7500 | 0.166 | 0.063249 | 0.070 | 1.026547 | 0.105 | 0.117713 | 0.047 | 0.850 | 716.61 | 1.5 | 717.20 | 0.54 | 717.39 | 0.32 |
| z6 | 4.9 | 173 | 0.347 | 20.6 | 4.1900 | 99.87% | 224 | 0.45 | 14203 | 0.107 | 0.063258 | 0.043 | 1.026774 | 0.088 | 0.117722 | 0.048 | 0.973 | 716.92 | 0.9 | 717.31 | 0.45 | 717.44 | 0.33 |
| z7 | 7.6 | 65 | 0.550 | 8.2 | 2.4040 | 99.57% | 72 | 0.85 | 4366 | 0.170 | 0.063238 | 0.095 | 1.027715 | 0.130 | 0.117867 | 0.051 | 0.795 | 716.24 | 2.0 | 717.78 | 0.67 | 718.28 | 0.35 |
| z8 | 2.2 | 136 | 0.595 | 17.5 | 1.4804 | 99.47% | 59 | 0.65 | 3510 | 0.184 | 0.063183 | 0.120 | 1.026096 | 0.158 | 0.117784 | 0.065 | 0.725 | 714.40 | 2.6 | 716.97 | 0.81 | 717.79 | 0.44 |
| z9 | 2.2 | 257 | 0.227 | 30.1 | 2.8028 | 99.45% | 51 | 1.28 | 3358 | 0.070 | 0.063200 | 0.132 | 1.026026 | 0.163 | 0.117745 | 0.053 | 0.683 | 714.96 | 2.8 | 716.94 | 0.84 | 717.57 | 0.36 |
| z10 | 1.5 | 267 | 0.633 | 34.7 | 1.9102 | 99.48% | 60 | 0.82 | 3568 | 0.195 | 0.063230 | 0.116 | 1.027382 | 0.151 | 0.117844 | 0.057 | 0.737 | 715.98 | 2.5 | 717.62 | 0.78 | 718.14 | 0.39 |
| **F840A** *(N64°42.431', W140°01.312')* | | | | | | | | | | | | | | | | | | | | | | | |
| z3 | 1.3 | 196 | 0.323 | 23.6 | 1.2472 | 99.30% | 42 | 0.72 | 2676 | 0.100 | 0.063131 | 0.152 | 1.019713 | 0.189 | 0.117147 | 0.071 | 0.661 | 712.65 | 3.2 | 713.77 | 0.97 | 714.12 | 0.48 |
| z5 | 1.7 | 317 | 0.388 | 38.1 | 2.6580 | 99.64% | 83 | 0.78 | 5203 | 0.120 | 0.063171 | 0.125 | 1.016726 | 0.125 | 0.116731 | 0.060 | 0.789 | 713.99 | 1.8 | 712.27 | 0.64 | 711.72 | 0.40 |
| z6 | 0.69 | 343 | 0.512 | 44.1 | 1.1586 | 98.75% | 24 | 1.21 | 1487 | 0.158 | 0.063081 | 0.310 | 1.021829 | 0.344 | 0.117485 | 0.068 | 0.573 | 710.95 | 6.6 | 714.83 | 1.77 | 716.07 | 0.46 |
| z8 | 0.60 | 256 | 0.446 | 33.6 | 0.7629 | 98.31% | 18 | 1.08 | 1099 | 0.140 | 0.065036 | 0.379 | 1.074841 | 0.450 | 0.119864 | 0.173 | 0.572 | 775.51 | 8.0 | 741.11 | 2.37 | 729.78 | 1.19 |
| z9 | 1.1 | 459 | 0.437 | 55.1 | 2.3611 | 99.67% | 91 | 0.64 | 5626 | 0.136 | 0.063161 | 0.085 | 1.002469 | 0.122 | 0.115112 | 0.055 | 0.788 | 713.66 | 1.8 | 705.06 | 0.62 | 702.37 | 0.37 |
| z10 | 0.92 | 350 | 0.417 | 34.8 | 1.2794 | 99.67% | 90 | 0.35 | 5572 | 0.136 | 0.063159 | 0.088 | 0.831078 | 0.133 | 0.095434 | 0.074 | 0.786 | 713.59 | 1.9 | 614.21 | 0.61 | 587.60 | 0.42 |
| z21 | 0.60 | 422 | 0.465 | 53.3 | 1.2484 | 99.03% | 31 | 1.00 | 1927 | 0.144 | 0.063244 | 0.207 | 1.025859 | 0.253 | 0.117643 | 0.094 | 0.631 | 716.45 | 4.4 | 716.85 | 1.30 | 716.98 | 0.64 |
| z22 | 0.69 | 490 | 0.406 | 59.9 | 1.6392 | 99.25% | 39 | 1.02 | 2473 | 0.126 | 0.063315 | 0.161 | 1.017949 | 0.193 | 0.116605 | 0.052 | 0.693 | 718.84 | 3.4 | 712.88 | 0.99 | 710.99 | 0.35 |
| z23 | 0.60 | 704 | 0.421 | 86.4 | 2.0517 | 99.39% | 49 | 1.03 | 3066 | 0.130 | 0.063262 | 0.137 | 1.022039 | 0.167 | 0.117172 | 0.050 | 0.691 | 717.05 | 2.9 | 714.94 | 0.86 | 714.27 | 0.34 |
| z24 | 0.46 | 368 | 0.462 | 46.5 | 0.8287 | 98.93% | 28 | 0.74 | 1742 | 0.143 | 0.063230 | 0.229 | 1.025504 | 0.272 | 0.117629 | 0.088 | 0.611 | 715.98 | 4.9 | 716.68 | 1.40 | 716.90 | 0.60 |
| z25 | 0.50 | 241 | 0.396 | 30.3 | 0.5965 | 98.53% | 20 | 0.73 | 1263 | 0.122 | 0.063105 | 0.319 | 1.022620 | 0.363 | 0.117531 | 0.086 | 0.606 | 711.76 | 6.8 | 715.23 | 1.87 | 716.34 | 0.58 |
| z28 | 0.46 | 265 | 0.589 | 35.1 | 0.5955 | 98.37% | 19 | 0.81 | 1141 | 0.182 | 0.063366 | 0.353 | 1.027428 | 0.410 | 0.117597 | 0.133 | 0.567 | 720.53 | 7.5 | 717.64 | 2.11 | 716.72 | 0.90 |
| z29 | 0.41 | 505 | 0.310 | 61.9 | 1.0196 | 98.59% | 20 | 1.20 | 1319 | 0.096 | 0.063311 | 0.322 | 1.022513 | 0.360 | 0.117135 | 0.064 | 0.661 | 718.70 | 6.8 | 715.18 | 1.85 | 714.05 | 0.43 |
| z30 | 0.46 | 311 | 0.329 | 38.9 | 0.7002 | 98.21% | 16 | 1.05 | 1038 | 0.102 | 0.063267 | 0.377 | 1.025276 | 0.421 | 0.117533 | 0.076 | 0.637 | 717.22 | 8.0 | 716.56 | 2.16 | 716.35 | 0.51 |
| **F834_147.5** *(N64°42', W139°51')* | | | | | | | | | | | | | | | | | | | | | | | |
| z1 | 8.4 | 298 | 0.668 | 43.5 | 13.9105 | 99.93% | 474 | 0.77 | 27610 | 0.206 | 0.066180 | 0.041 | 1.215305 | 0.085 | 0.133185 | 0.048 | 0.970 | 812.08 | 0.9 | 807.63 | 0.47 | 806.01 | 0.36 |
| z2 | 3.6 | 483 | 0.599 | 67.0 | 9.3940 | 99.86% | 218 | 1.11 | 12921 | 0.186 | 0.065966 | 0.090 | 1.164535 | 0.090 | 0.128036 | 0.046 | 0.933 | 805.29 | 1.1 | 784.08 | 0.49 | 776.65 | 0.34 |
| z3 | 4.4 | 147 | 0.570 | 21.2 | 3.6234 | 99.76% | 132 | 0.70 | 7886 | 0.175 | 0.066103 | 0.071 | 1.222788 | 0.107 | 0.134161 | 0.050 | 0.831 | 809.65 | 1.5 | 811.05 | 0.60 | 811.56 | 0.38 |
| z4 | 2.2 | 227 | 0.486 | 55.0 | 4.6614 | 99.75% | 122 | 0.97 | 7355 | 0.149 | 0.088094 | 0.066 | 2.740633 | 0.122 | 0.225634 | 0.083 | 0.859 | 1384.53 | 1.3 | 1339.55 | 0.91 | 1311.57 | 0.98 |
| z5 | 2.6 | 491 | 0.595 | 68.9 | 6.8215 | 99.78% | 145 | 1.21 | 8608 | 0.184 | 0.066006 | 0.061 | 1.178502 | 0.099 | 0.129494 | 0.047 | 0.886 | 806.56 | 1.3 | 790.62 | 0.54 | 784.98 | 0.35 |
| z6 | 1.4 | 203 | 0.599 | 30.2 | 1.5652 | 99.04% | 32 | 1.25 | 1930 | 0.184 | 0.066073 | 0.200 | 1.222218 | 0.247 | 0.134159 | 0.093 | 0.639 | 808.70 | 4.2 | 810.79 | 1.38 | 811.55 | 0.71 |
| z8 | 0.84 | 247 | 0.560 | 36.6 | 1.1645 | 98.91% | 28 | 1.06 | 1702 | 0.172 | 0.066062 | 0.228 | 1.221812 | 0.277 | 0.134138 | 0.104 | 0.621 | 808.34 | 4.8 | 810.60 | 1.55 | 811.43 | 0.79 |
| z9 | 3.0 | 133 | 0.560 | 19.4 | 2.2363 | 99.46% | 57 | 1.01 | 3418 | 0.172 | 0.066065 | 0.116 | 1.221903 | 0.151 | 0.134142 | 0.056 | 0.737 | 808.44 | 2.4 | 810.65 | 0.85 | 811.45 | 0.43 |
| **S8** *(N72°11.275', W111°45.549')* | | | | | | | | | | | | | | | | | | | | | | | |
| b1 | 0.09 | 509 | 0.079 | 61.1 | 0.2302 | 97.37% | 10 | 0.51 | 707 | 0.025 | 0.063560 | 0.555 | 1.023981 | 0.636 | 0.116844 | 0.176 | 0.571 | 727.02 | 11.8 | 715.91 | 3.27 | 712.37 | 1.19 |
| b2 | 0.09 | 672 | 0.098 | 79.0 | 0.2911 | 98.27% | 16 | 0.42 | 1078 | 0.030 | 0.063445 | 0.369 | 1.028663 | 0.429 | 0.117591 | 0.130 | 0.584 | 723.18 | 7.8 | 718.26 | 2.21 | 716.68 | 0.88 |
| b4 | 0.06 | 846 | 0.059 | 100.1 | 0.2566 | 97.82% | 12 | 0.47 | 853 | 0.018 | 0.063594 | 0.474 | 1.030432 | 0.543 | 0.117517 | 0.147 | 0.578 | 728.16 | 10.0 | 719.14 | 2.80 | 716.26 | 1.00 |
| b5 | 0.05 | 680 | 0.124 | 96.0 | 0.1699 | 93.05% | 4 | 1.04 | 267 | 0.038 | 0.063358 | 1.622 | 1.025140 | 1.622 | 0.117349 | 0.330 | 0.588 | 720.28 | 30.8 | 716.49 | 8.34 | 715.29 | 2.24 |
| b6 | 0.07 | 983 | 0.089 | 115.5 | 0.3195 | 98.24% | 15 | 0.47 | 1056 | 0.028 | 0.063298 | 0.387 | 1.025707 | 0.458 | 0.117526 | 0.170 | 0.575 | 718.25 | 8.2 | 716.78 | 2.36 | 716.31 | 1.15 |
| b7 | 0.07 | 611 | 0.183 | 76.6 | 0.1979 | 96.96% | 9 | 0.51 | 611 | 0.057 | 0.063110 | 0.860 | 1.018902 | 0.941 | 0.117094 | 0.249 | 0.445 | 711.93 | 18.3 | 713.36 | 4.82 | 713.82 | 1.68 |
| b8 | 0.08 | 335 | 0.087 | 47.6 | 0.1305 | 92.59% | 3 | 0.86 | 251 | 0.027 | 0.063243 | 1.638 | 1.023190 | 1.834 | 0.117340 | 0.404 | 0.569 | 716.40 | 34.8 | 715.52 | 9.42 | 715.24 | 2.74 |

(a) z1, b2 etc. are labels single zircon (z) or baddeleyite (b) grains or fragments; all zircon grains were annealed and chemically abraded after Mattinson (2005), baddeleyite needles were analyzed without abrasion.
(b) Nominal fraction weights estimated from photomicrographic grain dimensions, adjusted for partial dissolution during chemical abrasion.
(c) Nominal U and total Pb concentrations subject to uncertainty in photomicrographic estimation of weight and partial dissolution during chemical abrasion.
(d) Model Th/U ratio calculated from radiogenic 208Pb/206Pb ratio and 207Pb/235U age.
(e) Pb* and Pbc represent radiogenic and common Pb, respectively; mol % $^{206}Pb^*$ with respect to radiogenic, blank and initial common Pb.
(f) Measured ratio corrected for spike and fractionation only. Mass fractionation correction of 0.18 ± 0.02 (1-sigma) %/amu (atomic mass unit) was applied to all single-collector Daly analyses, based on analysis of NBS-981 and NBS-982.
(g) Corrected for fractionation, spike, and common Pb; all common Pb was assumed to be procedural blank: 206Pb/204Pb = 18.60 ± 0.80%; 207Pb/204Pb = 15.69 ± 0.32%; 208Pb/204Pb = 38.51 ± 0.74% (all uncertainties 1-sigma). 206Pb/238U and 207Pb/206Pb ages corrected for initial disequilibrium in 230Th/238U using Th/U [magma] = 3.
(h) Errors are 2-sigma, propagated using the algorithms of Schmitz and Schoene (2007).
(i) Calculations are based on the decay constants of Jaffey et al. (1971). 206Pb/238U and 207Pb/206Pb ages corrected for initial disequilibrium in 230Th/238U using Th/U [magma] = 3.

Table S2. Carbon and oxygen isotope data tables

Base of F833 at: N64°42.702', W139°50.074'

| section | height (m) | d13C | d18O | unit | cumulative thickness (m) |
|---|---|---|---|---|---|
| F833 | 1.0 | 1.58 | -5.67 | PF1a | 1.0 |
| F833 | 2.6 | 2.11 | -4.82 | PF1a | 2.6 |
| F833 | 3.2 | -0.13 | -6.42 | PF1a | 3.2 |
| F833 | 4.0 | -0.48 | -6.07 | PF1a | 4.0 |
| F833 | 5.0 | 0.08 | -6.35 | PF1a | 5.0 |
| F833 | 9.0 | 1.18 | -5.86 | PF1a | 9.0 |
| F833 | 11.4 | 0.81 | -6.63 | PF1a | 11.4 |
| F833 | 12.0 | 1.39 | -6.42 | PF1a | 12.0 |
| F833 | 13.0 | 1.48 | -6.27 | PF1a | 13.0 |
| F833 | 14.0 | 0.60 | -5.77 | PF1a | 14.0 |
| F833 | 15.0 | 1.64 | -6.20 | PF1a | 15.0 |
| F833 | 16.0 | 1.73 | -6.25 | PF1a | 16.0 |
| F833 | 17.0 | 1.42 | -5.79 | PF1a | 17.0 |
| F833 | 18.0 | 1.25 | -6.99 | PF1a | 18.0 |
| F833 | 19.0 | 1.15 | -8.14 | PF1a | 19.0 |
| F833 | 20.0 | 1.21 | -7.36 | PF1a | 20.0 |
| F833 | 21.1 | 1.19 | -6.34 | PF1a | 21.1 |
| F833 | 22.0 | 0.97 | -6.02 | PF1a | 22.0 |
| F833 | 23.0 | 0.77 | -6.25 | PF1a | 23.0 |
| F833 | 25.0 | 1.26 | -6.30 | PF1a | 25.0 |
| F833 | 27.0 | 1.34 | -6.03 | PF1a | 27.0 |
| F833 | 28.0 | 1.03 | -7.72 | PF1a | 28.0 |
| F833 | 29.0 | 1.44 | -6.68 | PF1a | 29.0 |
| F833 | 30.0 | 1.07 | -7.06 | PF1a | 30.0 |
| F833 | 31.0 | 0.95 | -6.51 | PF1a | 31.0 |
| F833 | 33.0 | 0.27 | -6.79 | PF1a | 33.0 |
| F833 | 34.0 | 0.12 | -5.93 | PF1a | 34.0 |
| F833 | 35.0 | 1.71 | -5.62 | PF1a | 35.0 |
| F833 | 36.3 | 0.34 | -7.45 | PF1a | 36.3 |
| F833 | 37.0 | 1.44 | -6.07 | PF1a | 37.0 |
| F833 | 38.0 | 0.73 | -6.73 | PF1a | 38.0 |
| F833 | 39.0 | -0.43 | -7.35 | PF1a | 39.0 |
| F833 | 40.0 | 1.05 | -6.58 | PF1a | 40.0 |
| F833 | 41.0 | -0.07 | -6.56 | PF1a | 41.0 |
| F833 | 44.0 | 0.62 | -6.86 | PF1a | 44.0 |
| F833 | 45.0 | 1.18 | -6.36 | PF1a | 45.0 |
| F833 | 46.0 | 0.71 | -5.86 | PF1a | 46.0 |
| F833 | 47.0 | 0.01 | -6.11 | PF1a | 47.0 |
| F833 | 49.0 | 0.25 | -6.71 | PF1a | 49.0 |
| F833 | 50.0 | 0.39 | -5.90 | PF1a | 50.0 |
| F833 | 51.1 | -0.33 | -6.13 | PF1a | 51.1 |
| F833 | 52.0 | 0.36 | -6.58 | PF1a | 52.0 |
| F833 | 53.0 | 0.57 | -6.57 | PF1a | 53.0 |
| F833 | 54.0 | -0.80 | -6.87 | PF1a | 54.0 |
| F833 | 55.0 | 0.63 | -5.81 | PF1a | 55.0 |
| F833 | 56.0 | -0.17 | -5.74 | PF1a | 56.0 |
| F833 | 57.0 | -0.32 | -6.16 | PF1a | 57.0 |
| F833 | 58.0 | -0.71 | -4.30 | PF1a | 58.0 |
| F833 | 59.0 | -0.46 | -5.32 | PF1a | 59.0 |
| F833 | 60.0 | -0.37 | -6.40 | PF1a | 60.0 |
| F833 | 60.8 | -0.70 | -6.01 | PF1a | 60.8 |
| F833 | 69.6 | 0.32 | -6.61 | PF1a | 69.6 |
| F833 | 70.5 | 1.38 | -6.65 | PF1a | 70.5 |
| F833 | 71.5 | 1.49 | -6.06 | PF1a | 71.5 |
| F833 | 88.2 | 0.41 | -5.97 | PF1a | 88.2 |
| F833 | 89.0 | 1.48 | -5.82 | PF1a | 89.0 |
| F833 | 90.0 | 1.37 | -5.44 | PF1a | 90.0 |
| F833 | 91.0 | 0.88 | -5.93 | PF1a | 91.0 |
| F833 | 92.0 | 1.16 | -5.97 | PF1a | 92.0 |
| F833 | 93.0 | 1.23 | -5.44 | PF1a | 93.0 |
| F833 | 94.0 | 1.25 | -5.67 | PF1a | 94.0 |
| F833 | 95.0 | 1.37 | -6.78 | PF1a | 95.0 |
| F833 | 96.0 | 1.23 | -5.67 | PF1a | 96.0 |
| F833 | 98.0 | 0.59 | -6.20 | PF1a | 98.0 |
| F833 | 106.6 | 0.93 | -5.81 | PF1a | 106.6 |
| F833 | 107.5 | 1.17 | -6.75 | PF1a | 107.5 |
| F833 | 115.0 | 1.42 | -6.81 | PF1a | 115.0 |
| F833 | 116.0 | 1.22 | -5.84 | PF1a | 116.0 |
| F833 | 117.0 | 0.62 | -6.19 | PF1a | 117.0 |
| F833 | 118.0 | 0.91 | -5.85 | PF1a | 118.0 |
| F833 | 119.6 | 1.15 | -6.77 | PF1a | 119.6 |
| F833 | 121.0 | 0.99 | -7.31 | PF1a | 121.0 |
| F833 | 122.0 | 1.46 | -7.06 | PF1a | 122.0 |
| F833 | 123.0 | 1.08 | -7.10 | PF1a | 123.0 |
| F833 | 124.0 | 1.39 | -6.58 | PF1a | 124.0 |
| F833 | 125.0 | 1.08 | -7.40 | PF1a | 125.0 |
| F833 | 126.0 | 1.77 | -5.92 | PF1a | 126.0 |
| F833 | 127.0 | 1.40 | -5.88 | PF1a | 127.0 |
| F833 | 128.0 | 1.40 | -6.46 | PF1a | 128.0 |
| F833 | 129.0 | 1.50 | -6.23 | PF1a | 129.0 |
| F833 | 130.0 | 1.39 | -6.48 | PF1a | 130.0 |
| F833 | 131.0 | 1.42 | -6.34 | PF1a | 131.0 |
| F833 | 132.0 | 1.32 | -6.47 | PF1a | 132.0 |
| F833 | 133.0 | 1.00 | -6.22 | PF1a | 133.0 |
| F833 | 134.0 | 1.46 | -6.47 | PF1a | 134.0 |
| F833 | 135.3 | 1.40 | -5.63 | PF1a | 135.3 |
| F833 | 136.0 | 1.53 | -5.68 | PF1a | 136.0 |
| F833 | 138.0 | -0.02 | -6.54 | PF1a | 138.0 |
| F833 | 139.0 | 0.26 | -6.53 | PF1a | 139.0 |
| F833 | 141.0 | 1.97 | -5.46 | PF1a | 141.0 |

| F833 | 143.0 | 3.31 | -4.18 | PF1a | 143.0 |
|------|-------|------|-------|------|-------|
| F833 | 144.0 | 1.28 | -4.61 | PF1a | 144.0 |
| F833 | 145.0 | 2.36 | -4.81 | PF1a | 145.0 |
| F833 | 145.9 | 1.18 | -5.90 | PF1a | 145.9 |
| F833 | 146.0 | 1.21 | -6.10 | PF1a | 146.0 |
| F833 | 147.0 | 1.67 | -5.92 | PF1a | 147.0 |
| F833 | 148.0 | 1.45 | -5.83 | PF1a | 148.0 |
| F833 | 150.0 | 1.55 | -5.87 | PF1a | 150.0 |
| F833 | 151.0 | 1.50 | -6.11 | PF1a | 151.0 |
| F833 | 151.8 | 2.02 | -5.19 | PF1a | 151.8 |
| F833 | 153.0 | 1.44 | -6.06 | PF1a | 153.0 |
| F833 | 154.0 | 1.55 | -6.02 | PF1a | 154.0 |
| F833 | 155.0 | 1.80 | -5.72 | PF1a | 155.0 |
| F833 | 157.0 | 1.64 | -6.09 | PF1a | 157.0 |
| F833 | 158.0 | 1.53 | -5.98 | PF1a | 158.0 |
| F833 | 159.0 | 1.75 | -5.82 | PF1a | 159.0 |
| F833 | 160.0 | 1.87 | -5.97 | PF1a | 160.0 |
| F833 | 161.0 | 1.96 | -5.78 | PF1a | 161.0 |
| F833 | 163.0 | 1.75 | -6.12 | PF1a | 163.0 |
| F833 | 163.2 | 1.73 | -5.95 | PF1a | 163.2 |
| F833 | 164.0 | 1.17 | -5.81 | PF1a | 164.0 |
| F833 | 165.0 | 1.47 | -5.97 | PF1a | 165.0 |
| F833 | 166.0 | 2.28 | -5.57 | PF1a | 166.0 |
| F833 | 168.0 | 0.69 | -6.23 | PF1a | 168.0 |
| F833 | 169.2 | 1.55 | -5.83 | PF1a | 169.2 |
| F833 | 169.8 | 1.15 | -6.95 | PF1a | 169.8 |
| F833 | 171.2 | 1.72 | -5.82 | PF1a | 171.2 |
| F833 | 172.0 | 1.84 | -6.51 | PF1a | 172.0 |
| F833 | 173.2 | 1.75 | -6.20 | PF1a | 173.2 |
| F833 | 174.0 | 1.74 | -5.77 | PF1a | 174.0 |
| F833 | 175.0 | 1.58 | -6.30 | PF1a | 175.0 |
| F833 | 176.0 | 1.98 | -5.59 | PF1a | 176.0 |
| F833 | 177.0 | 2.01 | -5.43 | PF1a | 177.0 |
| F833 | 178.0 | 2.12 | -5.77 | PF1a | 178.0 |
| F833 | 179.0 | 2.18 | -6.34 | PF1a | 179.0 |
| F833 | 180.0 | 1.97 | -6.11 | PF1a | 180.0 |
| F833 | 181.0 | 2.12 | -6.42 | PF1a | 181.0 |
| F833 | 182.0 | 2.07 | -6.24 | PF1a | 182.0 |
| F833 | 183.0 | 2.31 | -5.82 | PF1a | 183.0 |
| F833 | 184.0 | 2.04 | -6.03 | PF1a | 184.0 |
| F833 | 185.0 | 2.47 | -5.79 | PF1a | 185.0 |
| F833 | 186.0 | 3.81 | -4.83 | PF1a | 186.0 |
| F833 | 191.0 | 6.16 | -7.53 | PF1a | 191.0 |
| F833 | 200.0 | 5.49 | -7.45 | PF1a | 200.0 |
| F833 | 202.0 | 4.18 | -7.62 | PF1a | 202.0 |
| F833 | 203.0 | 2.94 | -5.18 | PF1a | 203.0 |
| F833 | 204.0 | 4.66 | -5.57 | PF1a | 204.0 |
| F833 | 205.0 | 4.79 | -7.50 | PF1a | 205.0 |
| F833 | 206.0 | 4.21 | -6.19 | PF1a | 206.0 |
| F833 | 207.0 | 4.16 | -6.01 | PF1a | 207.0 |
| F833 | 208.0 | 4.16 | -5.62 | PF1a | 208.0 |
| F833 | 209.0 | 4.89 | -5.86 | PF1a | 209.0 |
| F833 | 210.0 | 4.07 | -6.19 | PF1a | 210.0 |
| F833 | 211.0 | 5.30 | -5.76 | PF1a | 211.0 |
| F833 | 212.0 | 3.55 | -5.99 | PF1a | 212.0 |
| F833 | 215.2 | 2.73 | -6.55 | PF1a | 215.2 |
| F833 | 235.5 | 2.85 | -5.64 | PF1a | 235.5 |
| F833 | 236.0 | 3.06 | -5.60 | PF1a | 236.0 |
| F833 | 237.0 | 3.18 | -5.91 | PF1a | 237.0 |
| F833 | 238.5 | 3.58 | -5.70 | PF1a | 238.5 |
| F833 | 239.0 | 4.01 | -5.41 | PF1a | 239.0 |
| F833 | 240.0 | 3.31 | -5.45 | PF1a | 240.0 |
| F833 | 241.0 | 2.89 | -5.48 | PF1a | 241.0 |
| F833 | 242.0 | 3.07 | -5.32 | PF1a | 242.0 |
| F833 | 243.0 | 3.11 | -5.56 | PF1a | 243.0 |
| F833 | 244.0 | 2.93 | -5.82 | PF1a | 244.0 |
| F833 | 247.0 | 4.35 | -6.00 | PF1a | 247.0 |
| F833 | 248.0 | 3.53 | -1.69 | PF1a | 248.0 |
| F833 | 250.0 | 3.66 | -5.41 | PF1a | 250.0 |
| F833 | 251.0 | 2.79 | -5.52 | PF1a | 251.0 |
| F833 | 255.0 | 3.46 | -6.06 | PF1a | 255.0 |
| F833 | 256.0 | 3.02 | -5.31 | PF1a | 256.0 |
| F833 | 257.0 | 3.15 | -5.94 | PF1a | 257.0 |
| F833 | 313.0 | 6.05 | -4.79 | PF1a | 313.0 |
| F833 | 314.0 | 5.16 | -5.02 | PF1a | 314.0 |
| F833 | 323.5 | 6.34 | -4.52 | PF1a | 323.5 |
| F833 | 324.5 | 4.97 | -4.75 | PF1a | 324.5 |
| F833 | 325.3 | 4.23 | -4.87 | PF1a | 325.3 |
| F833 | 353.0 | 4.21 | -4.73 | PF1a | 353.0 |
| F833 | 355.0 | 5.73 | -4.24 | PF1a | 355.0 |
| F833 | 356.0 | 5.54 | -4.80 | PF1a | 356.0 |
| F833 | 357.0 | 6.10 | -3.74 | PF1a | 357.0 |
| F833 | 358.0 | 4.89 | -5.41 | PF1a | 358.0 |
| F833 | 359.0 | 4.70 | -5.34 | PF1a | 359.0 |
| F833 | 361.0 | 5.86 | -4.44 | PF1a | 361.0 |
| F833 | 362.0 | 5.41 | -4.05 | PF1a | 362.0 |
| F833 | 363.0 | 5.24 | -3.92 | PF1a | 363.0 |
| F833 | 364.0 | 5.22 | -5.43 | PF1a | 364.0 |
| F833 | 366.0 | 4.60 | -5.50 | PF1a | 366.0 |
| F833 | 367.0 | 5.54 | -4.84 | PF1a | 367.0 |
| F833 | 368.0 | 5.87 | -3.47 | PF1a | 368.0 |
| F833 | 369.0 | 5.34 | -5.54 | PF1a | 369.0 |

Table S2. Carbon and oxygen isotope data tables

| F833 | 370.0 | 6.30 | -5.99 | PF1a | 370.0 |
|---|---|---|---|---|---|
| F833 | 371.0 | 5.62 | -3.89 | PF1a | 371.0 |
| F833 | 374.0 | 5.96 | -3.62 | PF1a | 374.0 |
| F833 | 375.0 | 5.62 | -4.51 | PF1a | 375.0 |
| F833 | 376.0 | 5.79 | -5.22 | PF1a | 376.0 |
| F833 | 377.0 | 5.66 | -5.66 | PF1a | 377.0 |
| F833 | 378.0 | 6.15 | -4.98 | PF1a | 378.0 |
| F833 | 380.0 | 6.44 | -4.62 | PF1a | 380.0 |
| F833 | 381.0 | 6.05 | -5.14 | PF1a | 381.0 |
| F833 | 382.0 | 5.92 | -4.57 | PF1a | 382.0 |
| F833 | 383.0 | 6.00 | -5.33 | PF1a | 383.0 |
| F833 | 384.0 | 5.68 | -6.15 | PF1a | 384.0 |
| F833 | 385.0 | 5.76 | -6.07 | PF1a | 385.0 |
| F833 | 386.0 | 5.67 | -6.02 | PF1a | 386.0 |
| F833 | 387.0 | 5.96 | -4.89 | PF1a | 387.0 |
| F833 | 388.0 | 6.49 | -5.12 | PF1a | 388.0 |
| F833 | 389.0 | 7.12 | -3.08 | PF1a | 389.0 |
| F833 | 390.5 | 5.91 | -5.22 | PF1a | 390.5 |
| F833 | 391.5 | 7.52 | -5.21 | PF1a | 391.5 |
| F833 | 392.5 | 6.39 | -5.32 | PF1a | 392.5 |
| F833 | 393.0 | 7.54 | -5.24 | PF1a | 393.0 |
| F833 | 394.0 | 5.96 | -5.27 | PF1a | 394.0 |
| F833 | 395.0 | 6.64 | -5.36 | PF1a | 395.0 |
| F833 | 396.0 | 6.08 | -5.51 | PF1a | 396.0 |
| F833 | 397.0 | 6.60 | -5.63 | PF1a | 397.0 |
| F833 | 398.0 | 6.32 | -6.09 | PF1a | 398.0 |
| F833 | 399.0 | 6.39 | -5.45 | PF1a | 399.0 |
| F833 | 400.0 | 6.28 | -5.71 | PF1a | 400.0 |
| F833 | 401.0 | 6.80 | -5.75 | PF1a | 401.0 |
| F833 | 402.0 | 6.57 | -5.42 | PF1a | 402.0 |
| F833 | 403.0 | 6.23 | -5.67 | PF1a | 403.0 |
| F833 | 404.0 | 6.99 | -4.88 | PF1a | 404.0 |
| F833 | 405.0 | 6.88 | -2.90 | PF1a | 405.0 |
| F833 | 406.0 | 6.49 | -5.56 | PF1a | 406.0 |
| F833 | 407.0 | 6.98 | -4.56 | PF1a | 407.0 |
| F833 | 408.0 | 6.93 | -7.42 | PF1a | 408.0 |
| F833 | 409.0 | 5.12 | -5.32 | PF1a | 409.0 |

Base of F834 at: ~N64°42', W139°51'

| section | height (m) | d13C | d18O | unit | cumulative thickness (m) |
|---|---|---|---|---|---|
| F834 | 0.0 | 5.76 | -5.97 | PF1a | 394.0 |
| F834 | 1.0 | 6.12 | -3.14 | PF1a | 395.0 |
| F834 | 2.0 | 6.39 | -5.84 | PF1a | 396.0 |
| F834 | 3.0 | 6.13 | -5.99 | PF1a | 397.0 |
| F834 | 4.0 | 6.35 | -5.92 | PF1a | 398.0 |
| F834 | 6.0 | 6.71 | -6.25 | PF1a | 400.0 |
| F834 | 7.0 | 6.06 | -6.44 | PF1a | 401.0 |
| F834 | 8.0 | 6.11 | -6.76 | PF1a | 402.0 |
| F834 | 9.0 | 6.16 | -6.02 | PF1a | 403.0 |
| F834 | 10.0 | 6.12 | -6.14 | PF1a | 404.0 |
| F834 | 11.0 | 6.69 | -5.55 | PF1a | 405.0 |
| F834 | 12.0 | 6.38 | -5.68 | PF1a | 406.0 |
| F834 | 13.0 | 6.69 | -6.01 | PF1a | 407.0 |
| F834 | 14.0 | 6.89 | -3.32 | PF1a | 408.0 |
| F834 | 15.0 | 5.13 | -4.95 | PF1a | 409.0 |
| F834 | 16.0 | 6.39 | -4.55 | PF1a | 410.0 |
| F834 | 17.0 | 4.96 | -4.66 | PF1a | 411.0 |
| F834 | 18.0 | 4.07 | -5.06 | PF1a | 412.0 |
| F834 | 19.0 | 6.95 | -4.70 | PF1a | 413.0 |
| F834 | 20.0 | 6.33 | -4.35 | PF1a | 414.0 |
| F834 | 21.0 | 5.67 | -3.82 | PF1a | 415.0 |
| F834 | 22.0 | 6.87 | -2.41 | PF1a | 416.0 |
| F834 | 23.0 | 7.72 | -3.65 | PF1a | 417.0 |
| F834 | 24.0 | 7.30 | -2.89 | PF1a | 418.0 |
| F834 | 25.0 | 9.23 | -4.00 | PF1a | 419.0 |
| F834 | 26.0 | 8.07 | -5.42 | PF1a | 420.0 |
| F834 | 27.0 | 8.49 | -5.25 | PF1a | 421.0 |
| F834 | 28.0 | 6.89 | -5.57 | PF1a | 422.0 |
| F834 | 29.0 | 7.49 | -5.67 | PF1a | 423.0 |
| F834 | 30.0 | 7.78 | -5.85 | PF1a | 424.0 |
| F834 | 31.0 | 7.65 | -6.50 | PF1a | 425.0 |
| F834 | 32.5 | 7.39 | -5.53 | PF1a | 426.5 |
| F834 | 33.0 | 8.12 | -3.81 | PF1a | 427.0 |
| F834 | 34.0 | 9.02 | -4.15 | PF1a | 428.0 |
| F834 | 35.0 | 8.68 | -3.29 | PF1a | 429.0 |
| F834 | 36.0 | 7.50 | -6.10 | PF1a | 430.0 |
| F834 | 37.0 | 7.74 | -5.45 | PF1a | 431.0 |
| F834 | 44.0 | 8.30 | -6.81 | PF1a | 438.0 |
| F834 | 45.0 | 9.19 | -5.99 | PF1a | 439.0 |
| F834 | 46.0 | 8.75 | -5.88 | PF1a | 440.0 |
| F834 | 49.0 | 6.64 | -6.93 | PF1a | 443.0 |
| F834 | 50.0 | 7.84 | -7.26 | PF1a | 444.0 |
| F834 | 51.0 | 6.62 | -7.27 | PF1a | 445.0 |
| F834 | 52.0 | 6.58 | -7.32 | PF1a | 446.0 |
| F834 | 53.0 | 7.05 | -6.89 | PF1a | 447.0 |
| F834 | 54.0 | 6.84 | -6.62 | PF1a | 448.0 |
| F834 | 55.0 | 6.33 | -6.95 | PF1a | 449.0 |
| F834 | 56.0 | 6.72 | -7.05 | PF1a | 450.0 |
| F834 | 57.0 | 6.90 | -7.10 | PF1a | 451.0 |
| F834 | 58.0 | 6.72 | -6.55 | PF1a | 452.0 |
| F834 | 59.0 | 6.73 | -6.37 | PF1a | 453.0 |
| F834 | 60.0 | 6.05 | -8.08 | PF1a | 454.0 |

Table S2. Carbon and oxygen isotope data tables

| section | height (m) | d13C | d18O | unit | cumulative thickness (m) |
|---|---|---|---|---|---|
| F834 | 61.0 | 7.23 | -7.03 | PF1a | 455.0 |
| F834 | 62.0 | 6.32 | -7.48 | PF1a | 456.0 |
| F834 | 65.0 | 6.86 | -6.87 | PF1a | 459.0 |
| F834 | 66.0 | 6.62 | -7.34 | PF1a | 460.0 |
| F834 | 67.0 | 6.55 | -7.48 | PF1a | 461.0 |
| F834 | 68.0 | 6.56 | -7.54 | PF1a | 462.0 |
| F834 | 69.0 | 6.81 | -7.24 | PF1a | 463.0 |
| F834 | 70.0 | 6.56 | -6.72 | PF1a | 464.0 |
| F834 | 73.0 | 6.89 | -6.53 | PF1a | 467.0 |
| F834 | 74.0 | 5.60 | -5.55 | PF1a | 468.0 |
| F834 | 75.0 | 6.77 | -4.44 | PF1a | 469.0 |
| F834 | 76.0 | 7.34 | -6.21 | PF1a | 470.0 |
| F834 | 77.0 | 6.72 | -5.84 | PF1a | 471.0 |
| F834 | 78.0 | 7.56 | -4.21 | PF1a | 472.0 |
| F834 | 79.0 | 7.45 | -2.86 | PF1a | 473.0 |
| F834 | 80.0 | 7.19 | -6.77 | PF1a | 474.0 |
| F834 | 81.0 | 7.66 | -3.57 | PF1a | 475.0 |
| F834 | 82.0 | 7.31 | -10.78 | PF1a | 476.0 |
| F834 | 83.0 | 6.46 | -6.43 | PF1a | 477.0 |
| F834 | 84.0 | 6.98 | -6.52 | PF1a | 478.0 |
| F834 | 86.0 | 9.07 | -7.49 | PF1a | 480.0 |
| F834 | 87.0 | 8.93 | -6.26 | PF1a | 481.0 |
| F834 | 88.0 | 9.15 | -4.85 | PF1a | 482.0 |
| F834 | 89.0 | 9.49 | -6.29 | PF1a | 483.0 |
| F834 | 90.0 | 9.01 | -6.89 | PF1a | 484.0 |
| F834 | 91.0 | 9.51 | -6.34 | PF1a | 485.0 |
| F834 | 93.0 | 7.02 | -7.73 | PF1a | 487.0 |
| F834 | 94.0 | 6.63 | -5.61 | PF1a | 488.0 |
| F834 | 95.0 | 5.86 | -6.64 | PF1a | 489.0 |
| F834 | 96.0 | 6.83 | -6.94 | PF1a | 490.0 |
| F834 | 97.0 | 6.57 | -6.71 | PF1a | 491.0 |
| F834 | 98.0 | 6.49 | -6.52 | PF1a | 492.0 |
| F834 | 99.0 | 9.08 | -6.78 | PF1a | 493.0 |
| F834 | 100.0 | 9.39 | -7.20 | PF1a | 494.0 |
| F834 | 102.0 | 10.00 | -7.35 | PF1a | 496.0 |
| F834 | 104.0 | 8.77 | -7.63 | PF1a | 498.0 |
| F834 | 105.0 | 6.61 | -7.57 | PF1a | 499.0 |
| F834 | 116.0 | 5.20 | -3.79 | PF1a | 510.0 |
| F834 | 117.5 | 4.97 | -6.77 | PF1a | 511.5 |
| F834 | 123.0 | 6.70 | -0.18 | PF1a | 517.0 |
| F834 | 124.0 | 7.27 | -0.02 | PF1a | 518.0 |
| F834 | 125.0 | 7.07 | -0.67 | PF1a | 519.0 |
| F834 | 126.0 | 6.39 | -2.57 | PF1a | 520.0 |
| F834 | 127.0 | 7.30 | 0.23 | PF1a | 521.0 |
| F834 | 128.0 | 7.25 | -0.24 | PF1a | 522.0 |
| F834 | 129.0 | 6.99 | 0.41 | PF1a | 523.0 |
| F834 | 130.0 | 6.98 | 0.36 | PF1a | 524.0 |
| F834 | 131.0 | 7.33 | 0.85 | PF1a | 525.0 |
| F834 | 131.9 | 5.28 | -1.76 | PF1a | 525.9 |
| F834 | 133.0 | 6.15 | -2.57 | PF1a | 527.0 |
| F834 | 134.0 | 5.75 | -6.27 | PF1a | 528.0 |
| F834 | 135.0 | 6.30 | -1.94 | PF1a | 529.0 |
| F834 | 137.0 | 6.81 | -2.35 | PF1a | 531.0 |
| F834 | 139.0 | 7.32 | -0.27 | PF1a | 533.0 |
| F834 | 139.5 | 6.59 | -0.55 | PF1a | 533.5 |
| F834 | 141.0 | 6.84 | -0.04 | PF1a | 535.0 |
| F834 | 143.0 | 7.34 | -2.53 | PF1a | 537.0 |
| F834 | 145.0 | 6.83 | -1.48 | PF1a | 539.0 |
| F834 | 147.0 | 6.46 | 0.50 | PF1a | 541.0 |
| F834 | 171.0 | 6.72 | -5.10 | PF1a | 565.0 |
| F834 | 173.0 | 5.09 | -4.66 | PF1a | 567.0 |
| F834 | 178.0 | 5.97 | -5.05 | PF1a | 572.0 |
| F834 | 180.0 | 4.59 | -4.49 | PF1a | 574.0 |
| F834 | 182.0 | 4.78 | -2.07 | PF1a | 576.0 |
| F834 | 184.0 | 4.09 | -5.57 | PF1a | 578.0 |
| F834 | 186.0 | 4.32 | -5.91 | PF1a | 580.0 |
| F834 | 188.0 | 4.40 | -5.47 | PF1a | 582.0 |
| F834 | 190.0 | 4.66 | -5.46 | PF1a | 584.0 |
| F834 | 192.0 | 4.29 | -4.61 | PF1a | 586.0 |
| F834 | 198.0 | 4.14 | -5.94 | PF1a | 592.0 |
| F834 | 202.0 | 4.17 | -5.64 | PF1a | 596.0 |
| F834 | 206.0 | 3.92 | -6.16 | PF1a | 600.0 |
| F834 | 210.0 | 5.93 | -1.61 | PF1a | 604.0 |
| F834 | 213.0 | 5.49 | -3.90 | PF1a | 607.0 |
| F834 | 214.0 | 5.01 | -6.08 | PF1a | 608.0 |
| F834 | 216.0 | 5.39 | -2.13 | PF1a | 610.0 |
| F834 | 217.0 | 5.32 | -2.08 | PF1a | 611.0 |
| F834 | 218.0 | 3.84 | -1.12 | PF1a | 612.0 |
| F834 | 219.0 | 4.05 | -10.14 | PF1a | 613.0 |
| F834 | 224.0 | 4.18 | -10.02 | PF1a | 618.0 |
| F834 | 225.0 | 2.15 | -10.01 | PF1a | 619.0 |
| F834 | 226.0 | 2.80 | -10.41 | PF1a | 620.0 |
| F834 | 227.0 | 1.62 | -8.97 | PF1a | 621.0 |
| F834 | 228.0 | 1.43 | -9.95 | PF1a | 622.0 |
| F834 | 229.0 | 0.88 | -9.03 | PF1a | 623.0 |
| F834 | 230.0 | 1.53 | -10.79 | PF1a | 624.0 |

Base of F835 at:~N64°42', W139°51'

| section | height (m) | d13C | d18O | unit | cumulative thickness (m) |
|---|---|---|---|---|---|
| F835 | 65.0 | 0.12 | -3.90 | PF1a | 689.0 |
| F835 | 66.5 | 1.91 | -1.14 | PF1a | 690.5 |
| F835 | 68.2 | -1.91 | -2.98 | PF1a | 692.2 |

Table S2. Carbon and oxygen isotope data tables

| | | | | | |
|---|---|---|---|---|---|
| F835 | 69.4 | -1.96 | -4.23 | PF1a | 693.4 |
| F835 | 73.0 | -0.19 | -4.75 | PF1a | 697.0 |
| F835 | 74.0 | 1.11 | -2.83 | PF1a | 698.0 |
| F835 | 75.0 | 1.62 | -3.66 | PF1a | 699.0 |
| F835 | 76.0 | 1.21 | -3.89 | PF1a | 700.0 |
| F835 | 77.0 | 1.42 | -3.85 | PF1a | 701.0 |
| F835 | 78.0 | 1.19 | -4.33 | PF1a | 702.0 |
| F835 | 79.0 | 1.70 | -3.20 | PF1a | 703.0 |
| F835 | 80.0 | 1.98 | -4.07 | PF1a | 704.0 |
| F835 | 81.0 | 1.40 | -6.56 | PF1a | 705.0 |
| F835 | 83.0 | 1.42 | -4.91 | PF1a | 707.0 |
| F835 | 85.0 | 1.37 | -3.73 | PF1a | 709.0 |
| F835 | 87.0 | 2.36 | -3.75 | PF1a | 711.0 |
| F835 | 89.0 | 1.22 | -5.12 | PF1a | 713.0 |
| F835 | 91.0 | 1.19 | -3.51 | PF1a | 715.0 |
| F835 | 95.0 | 1.17 | -4.12 | PF1a | 719.0 |
| F835 | 97.0 | 1.71 | -3.97 | PF1a | 721.0 |
| F835 | 99.0 | 1.70 | -3.03 | PF1a | 723.0 |
| F835 | 101.0 | 1.15 | -4.11 | PF1a | 725.0 |
| F835 | 103.0 | 1.09 | -3.98 | PF1a | 727.0 |
| F835 | 104.0 | 0.40 | -4.31 | PF1a | 728.0 |
| F835 | 105.0 | -1.33 | -5.18 | PF1a | 729.0 |
| F835 | 106.0 | -2.02 | -5.10 | PF1a | 730.0 |
| F835 | 107.0 | -2.82 | -5.45 | PF1a | 731.0 |
| F835 | 111.0 | -0.44 | -2.35 | PF1 | 735.0 |
| F835 | 112.0 | -0.73 | -2.99 | PF1 | 736.0 |
| F835 | 113.0 | -1.00 | -2.80 | PF1 | 737.0 |
| F835 | 115.0 | -1.31 | -2.47 | PF1 | 739.0 |
| F835 | 117.0 | -0.80 | -2.61 | PF1 | 741.0 |
| F835 | 119.0 | 0.42 | -2.90 | PF1 | 743.0 |
| F835 | 121.0 | 0.51 | -3.10 | PF1 | 745.0 |
| F835 | 125.0 | -0.11 | -3.05 | PF1 | 749.0 |
| F835 | 129.0 | -0.04 | -3.53 | PF1 | 753.0 |
| F835 | 131.0 | -0.04 | -2.81 | PF1 | 755.0 |
| F835 | 133.0 | -0.28 | -3.55 | PF1 | 757.0 |
| F835 | 144.0 | 0.63 | -2.40 | PF1 | 768.0 |
| F835 | 146.0 | 0.50 | -2.62 | PF1 | 770.0 |
| F835 | 150.0 | -0.21 | -3.00 | PF1 | 774.0 |
| F835 | 154.0 | 0.86 | -2.78 | PF1 | 778.0 |
| F835 | 156.0 | 0.19 | -3.46 | PF1 | 780.0 |
| F835 | 158.0 | 0.49 | -3.30 | PF1 | 782.0 |
| F835 | 162.0 | 0.47 | -2.84 | PF1 | 786.0 |
| F835 | 164.0 | 0.51 | -3.08 | PF1 | 788.0 |
| F835 | 165.0 | 0.13 | -4.70 | PF1 | 789.0 |
| F835 | 170.0 | 0.40 | -4.21 | PF1 | 794.0 |
| F835 | 174.0 | -0.10 | -4.03 | PF1 | 798.0 |
| F835 | 176.0 | 0.53 | -3.33 | PF1 | 800.0 |
| F835 | 178.0 | 0.10 | -3.14 | PF1 | 802.0 |
| F835 | 180.0 | 0.69 | -3.04 | PF1 | 804.0 |
| F835 | 182.0 | 0.45 | -3.08 | PF1 | 806.0 |
| F835 | 184.0 | 0.44 | -4.85 | PF1 | 808.0 |
| F835 | 186.0 | 0.70 | -3.65 | PF1 | 810.0 |
| F835 | 190.0 | 0.48 | -3.97 | PF1 | 814.0 |
| F835 | 194.0 | 0.64 | -4.80 | PF1 | 818.0 |
| F835 | 196.0 | 0.81 | -4.18 | PF1 | 820.0 |
| F835 | 200.0 | -0.28 | -3.28 | PF1 | 824.0 |
| F835 | 202.0 | 0.46 | -3.59 | PF1 | 826.0 |
| F835 | 204.0 | 0.25 | -5.00 | PF1 | 828.0 |
| F835 | 206.0 | -0.02 | -4.83 | PF1 | 830.0 |
| F835 | 210.0 | 0.14 | -3.62 | PF1 | 834.0 |
| F835 | 212.0 | 0.19 | -5.13 | PF1 | 836.0 |
| F835 | 214.0 | 0.33 | -5.75 | PF1 | 838.0 |
| F835 | 216.0 | 0.68 | -4.32 | PF1 | 840.0 |
| F835 | 218.0 | 0.37 | -5.12 | PF1 | 842.0 |
| F835 | 223.0 | 0.53 | -4.55 | PF1 | 847.0 |
| F835 | 230.0 | 0.61 | -4.04 | PF1 | 854.0 |
| F835 | 233.0 | 0.76 | -3.83 | PF1 | 857.0 |
| F835 | 239.0 | 0.05 | -3.28 | PF1 | 863.0 |
| F835 | 241.0 | -0.48 | -2.80 | PF1 | 865.0 |
| F835 | 243.0 | -0.42 | -2.62 | PF1 | 867.0 |
| F835 | 245.5 | -0.08 | -3.39 | PF1 | 869.5 |
| F835 | 250.0 | -0.27 | -3.89 | PF1 | 874.0 |
| F835 | 254.0 | 0.52 | -5.59 | PF1 | 878.0 |
| F835 | 256.0 | 0.19 | -4.64 | PF1 | 880.0 |
| F835 | 260.0 | -0.28 | -4.84 | PF1 | 884.0 |
| F835 | 262.1 | -0.31 | -8.26 | PF1 | 886.1 |
| F835 | 264.0 | 0.32 | -3.62 | PF1 | 888.0 |
| F835 | 266.0 | 0.80 | -3.02 | PF1 | 890.0 |
| F835 | 268.0 | -0.12 | -3.70 | PF1 | 892.0 |
| F835 | 270.0 | -0.09 | -5.33 | PF1 | 894.0 |
| F835 | 272.0 | 0.65 | -3.82 | PF1 | 896.0 |
| F835 | 276.0 | 0.15 | -7.06 | PF1 | 900.0 |
| F835 | 278.0 | -0.21 | -3.13 | PF1 | 902.0 |
| F835 | 280.0 | 0.63 | -3.94 | PF1 | 904.0 |
| F835 | 284.0 | 0.02 | -4.74 | PF1 | 908.0 |
| F835 | 286.0 | 0.24 | -5.60 | PF1 | 910.0 |
| F835 | 288.0 | 0.11 | -3.40 | PF1 | 912.0 |
| F835 | 292.0 | 0.14 | -3.18 | PF1 | 916.0 |
| F835 | 294.0 | 0.49 | -4.57 | PF1 | 918.0 |
| F835 | 296.0 | 0.71 | -3.37 | PF1 | 920.0 |
| F835 | 298.0 | 0.39 | -3.96 | PF1 | 922.0 |
| F835 | 300.0 | 1.53 | -4.45 | PF1 | 924.0 |

Table S2. Carbon and oxygen isotope data tables

| section | height (m) | d13C | d18O | unit | cumulative thickness (m) |
|---|---|---|---|---|---|
| F835 | 302.0 | 0.27 | -3.91 | PF1 | 926.0 |
| F835 | 304.0 | 0.80 | -4.28 | PF1 | 928.0 |
| F835 | 306.0 | 0.70 | -3.31 | PF1 | 930.0 |
| F835 | 308.0 | 1.14 | -4.06 | PF1 | 932.0 |
| F835 | 312.0 | 0.15 | -4.47 | PF1 | 936.0 |

Base of F836 at:N64°41.806', W139°51.802'

| section | height (m) | d13C | d18O | unit | cumulative thickness (m) |
|---|---|---|---|---|---|
| F836 | 0.3 | 3.27 | -2.75 | PF1 | 940.3 |
| F836 | 2.0 | 1.81 | -2.16 | PF1 | 942.0 |
| F836 | 4.0 | 1.81 | -2.33 | PF1 | 944.0 |
| F836 | 6.0 | 1.38 | -2.91 | PF1 | 946.0 |
| F836 | 8.0 | 2.04 | -2.67 | PF1 | 948.0 |
| F836 | 10.0 | 1.97 | -3.10 | PF1 | 950.0 |
| F836 | 12.0 | 1.61 | -3.71 | PF1 | 952.0 |
| F836 | 14.0 | 1.80 | -2.62 | PF1 | 954.0 |
| F836 | 16.0 | 0.96 | -5.94 | PF1 | 956.0 |
| F836 | 18.0 | 1.67 | -2.93 | PF1 | 958.0 |
| F836 | 20.0 | 2.84 | -3.10 | PF1 | 960.0 |
| F836 | 22.0 | 1.82 | -2.96 | PF1 | 962.0 |
| F836 | 24.0 | 2.36 | -2.83 | PF1 | 964.0 |
| F836 | 26.0 | 2.64 | -3.53 | PF1 | 966.0 |
| F836 | 28.0 | 2.78 | -3.12 | PF1 | 968.0 |
| F836 | 30.0 | 1.75 | -3.04 | PF1 | 970.0 |
| F836 | 32.0 | 1.83 | -2.33 | PF1 | 972.0 |
| F836 | 34.0 | 2.35 | -4.98 | PF1 | 974.0 |
| F836 | 36.0 | 1.38 | -1.72 | PF1 | 976.0 |
| F836 | 38.0 | 3.29 | -1.12 | PF1 | 978.0 |
| F836 | 40.0 | 1.98 | -2.49 | PF1 | 980.0 |
| F836 | 42.0 | 2.74 | -1.60 | PF1 | 982.0 |
| F836 | 44.0 | 3.20 | -1.94 | PF1 | 984.0 |
| F836 | 46.0 | 1.60 | -1.75 | PF1 | 986.0 |
| F836 | 48.0 | 3.37 | -2.49 | PF1 | 988.0 |
| F836 | 50.0 | 2.92 | -2.32 | PF1 | 990.0 |
| F836 | 52.0 | 2.24 | -2.22 | PF1 | 992.0 |
| F836 | 54.0 | 2.95 | -1.38 | PF1 | 994.0 |
| F836 | 56.0 | 2.18 | -3.10 | PF1 | 996.0 |
| F836 | 58.0 | 2.33 | -2.25 | PF1 | 998.0 |
| F836 | 60.0 | 1.54 | -1.20 | PF1 | 1000.0 |
| F836 | 62.0 | 4.58 | -0.62 | PF1 | 1002.0 |
| F836 | 64.0 | 3.61 | -1.67 | PF1 | 1004.0 |
| F836 | 68.0 | 3.21 | -1.58 | PF1 | 1008.0 |
| F836 | 72.0 | 2.60 | -2.17 | PF1 | 1012.0 |
| F836 | 76.0 | 2.07 | -1.80 | PF1 | 1016.0 |
| F836 | 78.0 | 2.37 | -3.49 | PF1 | 1018.0 |
| F836 | 80.0 | 4.11 | -3.67 | PF1 | 1020.0 |
| F836 | 82.0 | 3.28 | -2.08 | PF1 | 1022.0 |
| F836 | 84.0 | 2.50 | -2.13 | PF1 | 1024.0 |
| F836 | 86.0 | 2.79 | -2.07 | PF1 | 1026.0 |
| F836 | 88.0 | 2.48 | -4.19 | PF1 | 1028.0 |
| F836 | 90.0 | 2.90 | -3.68 | PF1 | 1030.0 |
| F836 | 92.0 | 2.72 | -2.31 | PF1 | 1032.0 |
| F836 | 94.0 | 3.41 | -2.59 | PF1 | 1034.0 |
| F836 | 96.0 | 2.29 | -3.62 | PF1 | 1036.0 |
| F836 | 98.0 | 3.23 | -1.76 | PF1 | 1038.0 |
| F836 | 100.0 | 4.22 | -2.01 | PF1 | 1040.0 |
| F836 | 102.0 | 3.07 | -2.92 | PF1 | 1042.0 |
| F836 | 104.0 | 4.27 | -0.76 | PF1 | 1044.0 |
| F836 | 106.0 | 3.12 | -2.37 | PF1 | 1046.0 |
| F836 | 108.0 | 1.78 | -6.54 | PF1 | 1048.0 |
| F836 | 112.0 | 2.92 | -3.16 | PF1 | 1052.0 |
| F836 | 114.0 | 3.16 | -3.99 | PF1 | 1054.0 |
| F836 | 116.0 | 2.75 | -4.07 | PF1 | 1056.0 |
| F836 | 118.0 | 3.56 | -1.80 | PF1 | 1058.0 |
| F836 | 120.0 | 4.09 | -3.55 | PF1 | 1060.0 |
| F836 | 122.0 | 4.26 | -3.13 | PF1 | 1062.0 |
| F836 | 124.0 | 2.88 | -4.86 | PF1 | 1064.0 |
| F836 | 128.0 | 3.79 | -2.43 | PF1 | 1068.0 |
| F836 | 130.0 | 2.10 | -4.33 | PF1 | 1070.0 |
| F836 | 132.0 | 2.52 | -3.40 | PF1 | 1072.0 |
| F836 | 134.0 | 3.04 | -5.53 | PF1 | 1074.0 |
| F836 | 142.0 | 3.29 | -4.62 | PF1 | 1082.0 |
| F836 | 148.0 | 2.74 | -4.17 | PF1 | 1088.0 |
| F836 | 152.0 | 3.14 | -3.19 | PF1 | 1092.0 |
| F836 | 156.0 | 3.20 | -2.64 | PF1 | 1096.0 |
| F836 | 160.0 | 2.53 | -5.17 | PF1 | 1100.0 |
| F836 | 164.0 | 3.03 | -4.57 | PF1 | 1104.0 |
| F836 | 166.0 | 2.51 | -2.35 | PF1 | 1106.0 |
| F836 | 170.0 | 3.76 | -2.55 | PF1 | 1110.0 |
| F836 | 172.0 | 3.96 | -1.39 | PF1 | 1112.0 |
| F836 | 174.0 | 3.15 | -2.18 | PF1 | 1114.0 |
| F836 | 176.0 | 4.20 | -3.02 | PF1 | 1116.0 |
| F836 | 178.0 | 2.70 | -6.29 | PF1 | 1118.0 |
| F836 | 180.0 | 3.13 | -5.49 | PF1 | 1120.0 |
| F836 | 182.0 | 2.69 | -2.77 | PF1 | 1122.0 |
| F836 | 184.0 | 3.96 | -1.71 | PF1 | 1124.0 |
| F836 | 186.0 | 4.29 | -5.97 | PF1 | 1126.0 |
| F836 | 188.0 | 5.12 | -1.24 | PF1 | 1128.0 |
| F836 | 190.0 | 3.03 | -3.23 | PF1 | 1130.0 |
| F836 | 192.0 | 5.60 | -2.95 | PF1 | 1132.0 |
| F836 | 194.0 | 4.59 | -2.30 | PF1 | 1134.0 |
| F836 | 196.0 | 3.60 | -5.62 | PF1 | 1136.0 |

Table S2. Carbon and oxygen isotope data tables

| | | | | | |
|---|---|---|---|---|---|
| F836 | 198.0 | 4.94 | -2.69 | PF1 | 1138.0 |
| F836 | 200.0 | 3.91 | -0.80 | PF1 | 1140.0 |
| F836 | 202.0 | 3.83 | -2.55 | PF1 | 1142.0 |
| F836 | 204.0 | 5.14 | -1.77 | PF1 | 1144.0 |
| F836 | 206.0 | 3.88 | -2.78 | PF1 | 1146.0 |
| F836 | 208.0 | 4.18 | -0.99 | PF1 | 1148.0 |
| F836 | 210.0 | 5.40 | -1.79 | PF1 | 1150.0 |
| F836 | 212.0 | 3.70 | -4.78 | PF1 | 1152.0 |
| F836 | 214.0 | 3.80 | -1.78 | PF1 | 1154.0 |
| F836 | 218.0 | 4.28 | -2.53 | PF1 | 1158.0 |
| F836 | 220.0 | 4.00 | -2.57 | PF1 | 1160.0 |
| F836 | 224.0 | 5.06 | 0.29 | PF1 | 1164.0 |
| F836 | 226.0 | 4.08 | -2.80 | PF1 | 1166.0 |
| F836 | 230.0 | 4.76 | -2.65 | PF1 | 1170.0 |
| F836 | 232.0 | 4.47 | -2.01 | PF1 | 1172.0 |
| F836 | 238.0 | 5.19 | -2.36 | PF1 | 1178.0 |
| F836 | 240.0 | 5.16 | -1.79 | PF1 | 1180.0 |
| F836 | 242.0 | 6.05 | -1.64 | PF1 | 1182.0 |
| F836 | 246.0 | 4.81 | -1.95 | PF1 | 1186.0 |
| F836 | 248.0 | 6.08 | -2.42 | PF1 | 1188.0 |
| F836 | 250.0 | 5.39 | -2.25 | PF1 | 1190.0 |
| F836 | 252.0 | 4.03 | -3.85 | PF1 | 1192.0 |
| F836 | 258.0 | 5.62 | -2.07 | PF1 | 1198.0 |
| F836 | 260.0 | 4.86 | -2.01 | PF1 | 1200.0 |
| F836 | 264.0 | 5.21 | -1.86 | PF1 | 1204.0 |
| F836 | 266.0 | 5.90 | -1.08 | PF1 | 1206.0 |
| F836 | 268.0 | 4.94 | -2.68 | PF1 | 1208.0 |
| F836 | 270.0 | 4.12 | -2.53 | PF1 | 1210.0 |
| F836 | 272.0 | 5.75 | 0.33 | PF1 | 1212.0 |
| F836 | 274.0 | 2.60 | -1.39 | PF1 | 1214.0 |
| F836 | 276.0 | 4.80 | -2.83 | PF1 | 1216.0 |
| F836 | 278.0 | 4.00 | -3.99 | PF1 | 1218.0 |
| F836 | 293.0 | 5.46 | -4.98 | PF1 | 1233.0 |
| F836 | 296.0 | 5.84 | -2.20 | PF1 | 1236.0 |
| F836 | 298.0 | 5.73 | -1.93 | PF1 | 1238.0 |
| F836 | 304.0 | 5.56 | -2.01 | PF1 | 1244.0 |
| F836 | 308.0 | 5.52 | -2.61 | PF1 | 1248.0 |
| F836 | 312.0 | 5.56 | -3.25 | PF1 | 1252.0 |
| F836 | 316.0 | 6.28 | -1.41 | PF1 | 1256.0 |
| F836 | 333.0 | 6.62 | -2.01 | PF1 | 1273.0 |
| F836 | 340.0 | 6.37 | -2.16 | PF1 | 1280.0 |
| F836 | 352.0 | 5.84 | -1.39 | PF1 | 1292.0 |
| F836 | 354.0 | 6.81 | -1.05 | PF1 | 1294.0 |
| F836 | 358.0 | 5.97 | -1.67 | PF1 | 1298.0 |
| F836 | 364.0 | 6.24 | -1.69 | PF1 | 1304.0 |
| F836 | 366.0 | 6.24 | -1.27 | PF1 | 1306.0 |
| F836 | 368.0 | 6.88 | -1.17 | PF1 | 1308.0 |
| F836 | 370.0 | 7.02 | -1.71 | PF1 | 1310.0 |
| F836 | 372.0 | 7.10 | -1.47 | PF1 | 1312.0 |
| F836 | 374.0 | 6.86 | -1.11 | PF1 | 1314.0 |
| F836 | 376.0 | 6.99 | -0.43 | PF1 | 1316.0 |
| F836 | 378.0 | 6.09 | 0.79 | PF1 | 1318.0 |
| F836 | 380.0 | 6.98 | -1.70 | PF1 | 1320.0 |
| F836 | 382.0 | 6.18 | -0.61 | PF1 | 1322.0 |
| F836 | 394.0 | 6.28 | -1.29 | PF1 | 1334.0 |
| F836 | 399.0 | 3.27 | 1.33 | PF1 | 1339.0 |
| F836 | 501.0 | 1.97 | -3.83 | PF2 | 1441.0 |
| F836 | 503.0 | 1.52 | -3.19 | PF2 | 1443.0 |
| F836 | 505.0 | 1.90 | -4.34 | PF2 | 1445.0 |
| F836 | 507.0 | 3.22 | -3.17 | PF3 | 1447.0 |
| F836 | 509.0 | 3.69 | -0.65 | PF3 | 1449.0 |
| F836 | 511.0 | 3.17 | -1.56 | PF3 | 1451.0 |
| F836 | 513.0 | 3.59 | -3.28 | PF3 | 1453.0 |
| F836 | 515.0 | 4.53 | -0.75 | PF3 | 1455.0 |
| F836 | 519.0 | 2.79 | 1.68 | PF3 | 1459.0 |
| F836 | 523.0 | 5.01 | 0.41 | PF3 | 1463.0 |
| F836 | 527.0 | 4.63 | -0.52 | PF3 | 1467.0 |
| F836 | 531.0 | 2.97 | 0.18 | PF3 | 1471.0 |
| F836 | 535.0 | 4.50 | -3.54 | PF3 | 1475.0 |
| F836 | 539.0 | 3.36 | -1.56 | PF3 | 1479.0 |
| F836 | 543.0 | 3.99 | -3.31 | PF3 | 1483.0 |
| F836 | 547.0 | 4.14 | -0.94 | PF3 | 1487.0 |
| F836 | 551.0 | 3.92 | -0.61 | PF3 | 1491.0 |
| F836 | 555.0 | 4.58 | -1.08 | PF3 | 1495.0 |
| F836 | 557.0 | 5.63 | 0.25 | PF3 | 1497.0 |
| F836 | 559.0 | 5.00 | -0.60 | PF3 | 1499.0 |
| F836 | 563.0 | 4.06 | -2.64 | PF3 | 1503.0 |
| F836 | 567.0 | 3.62 | 1.67 | PF3 | 1507.0 |
| F836 | 571.0 | 3.60 | -1.09 | PF3 | 1511.0 |
| F836 | 575.0 | 2.06 | 0.98 | PF3 | 1515.0 |
| F836 | 576.0 | 2.80 | 1.43 | PF3 | 1516.0 |
| F836 | 586.0 | 3.66 | -0.37 | PF3 | 1526.0 |
| F836 | 587.0 | 4.94 | -4.87 | PF3 | 1527.0 |
| F836 | 591.0 | 4.42 | 2.66 | PF3 | 1531.0 |
| F836 | 595.0 | 4.38 | 0.35 | PF3 | 1535.0 |
| F836 | 599.0 | 4.77 | 0.79 | PF3 | 1539.0 |
| F836 | 603.0 | 3.87 | 0.21 | PF3 | 1543.0 |
| F836 | 609.0 | 4.54 | 1.58 | PF3 | 1549.0 |
| F836 | 613.0 | 4.52 | -0.23 | PF3 | 1553.0 |
| F836 | 617.0 | 4.90 | 1.18 | PF3 | 1557.0 |
| F836 | 621.0 | 5.37 | 1.38 | PF3 | 1561.0 |
| F836 | 625.0 | 5.00 | 2.41 | PF3 | 1565.0 |

| | | | | | |
|---|---|---|---|---|---|
| F836 | 629.0 | 5.11 | 1.47 | PF3 | 1569.0 |
| F836 | 631.0 | 5.04 | 2.16 | PF3 | 1571.0 |
| F836 | 633.0 | 4.53 | -3.29 | PF3 | 1573.0 |
| F836 | 635.0 | 4.75 | 0.37 | PF3 | 1575.0 |
| F836 | 637.0 | 4.60 | -1.10 | PF3 | 1577.0 |
| F836 | 639.0 | 4.65 | 0.91 | PF3 | 1579.0 |
| F836 | 641.0 | 5.18 | 1.51 | PF3 | 1581.0 |
| F836 | 643.0 | 5.88 | 2.62 | PF3 | 1583.0 |
| F836 | 645.0 | 5.43 | 1.57 | PF3 | 1585.0 |
| F836 | 647.0 | 5.62 | 1.67 | PF3 | 1587.0 |
| F836 | 649.0 | 5.81 | 2.53 | PF3 | 1589.0 |
| F836 | 651.0 | 5.35 | -0.03 | PF3 | 1591.0 |
| F836 | 659.0 | 5.19 | 1.66 | PF3 | 1599.0 |
| F836 | 661.0 | 5.67 | 1.05 | PF3 | 1601.0 |
| F836 | 663.0 | 5.52 | 0.64 | PF3 | 1603.0 |
| F836 | 665.0 | 5.63 | -0.78 | PF3 | 1605.0 |
| F836 | 667.0 | 5.20 | -0.24 | PF3 | 1607.0 |
| F836 | 671.0 | 5.37 | 0.30 | PF3 | 1611.0 |
| F836 | 673.0 | 5.18 | 0.17 | PF3 | 1613.0 |
| F836 | 677.0 | 4.14 | -0.01 | PF3 | 1617.0 |
| F836 | 679.0 | 4.29 | -1.13 | PF3 | 1619.0 |
| F836 | 681.0 | 3.95 | 0.62 | PF3 | 1621.0 |
| F836 | 683.0 | 4.38 | -2.49 | PF3 | 1623.0 |
| F836 | 685.0 | 4.90 | 0.87 | PF3 | 1625.0 |
| F836 | 687.0 | 4.47 | 0.18 | PF3 | 1627.0 |
| F836 | 689.0 | 4.38 | 0.08 | PF3 | 1629.0 |
| F836 | 691.0 | 4.86 | 0.55 | PF3 | 1631.0 |
| F836 | 693.0 | 4.70 | -2.95 | PF3 | 1633.0 |
| F836 | 697.0 | 2.20 | -0.89 | PF3 | 1637.0 |
| F836 | 699.0 | 4.75 | -1.70 | PF3 | 1639.0 |
| F836 | 701.0 | 4.71 | -2.84 | PF3 | 1641.0 |
| F836 | 705.0 | 4.90 | -0.51 | PF3 | 1645.0 |
| F836 | 707.0 | 5.13 | -0.69 | PF3 | 1647.0 |
| F836 | 709.0 | 4.86 | -4.20 | PF3 | 1649.0 |
| F836 | 711.0 | 4.86 | -0.22 | PF3 | 1651.0 |
| F836 | 713.0 | 4.37 | 0.03 | PF3 | 1653.0 |
| F836 | 717.0 | 3.17 | 1.09 | PF3 | 1657.0 |
| F836 | 720.0 | 3.27 | 0.24 | PF3 | 1660.0 |
| F836 | 726.0 | 3.44 | -2.88 | PF3 | 1666.0 |
| F836 | 728.0 | 4.07 | -0.87 | PF3 | 1668.0 |
| F836 | 730.0 | 3.59 | -1.56 | PF3 | 1670.0 |
| F836 | 732.0 | 3.36 | 1.57 | PF3 | 1672.0 |
| F836 | 734.0 | 3.61 | 1.21 | PF3 | 1674.0 |
| F836 | 736.0 | 4.08 | 1.85 | PF3 | 1676.0 |
| F836 | 738.0 | 4.12 | 1.46 | PF3 | 1678.0 |
| F836 | 740.0 | 4.01 | 0.80 | PF3 | 1680.0 |
| F836 | 742.0 | 3.92 | 2.36 | PF3 | 1682.0 |
| F836 | 744.0 | 3.39 | 2.00 | PF3 | 1684.0 |
| F836 | 746.0 | 3.16 | -1.04 | PF3 | 1686.0 |
| F836 | 748.0 | 3.68 | -2.17 | PF3 | 1688.0 |
| F836 | 750.0 | 3.08 | -0.77 | PF3 | 1690.0 |
| F836 | 752.0 | 3.83 | -1.06 | PF3 | 1692.0 |
| F836 | 754.0 | 3.81 | -2.81 | PF3 | 1694.0 |
| F836 | 756.0 | 3.98 | -2.72 | PF3 | 1696.0 |
| F836 | 758.0 | 4.09 | -4.68 | PF3 | 1698.0 |
| F836 | 760.0 | 4.00 | -1.65 | PF3 | 1700.0 |
| F836 | 762.0 | 4.02 | -3.97 | PF3 | 1702.0 |
| F836 | 764.0 | 4.17 | -0.57 | PF3 | 1704.0 |
| F836 | 766.0 | 3.79 | -4.07 | PF3 | 1706.0 |
| F836 | 768.0 | 3.91 | -2.88 | PF3 | 1708.0 |
| F836 | 770.0 | 4.02 | -1.27 | PF3 | 1710.0 |
| F836 | 772.0 | 3.95 | -3.15 | PF3 | 1712.0 |
| F836 | 774.0 | 3.70 | -3.95 | PF3 | 1714.0 |
| F836 | 776.0 | 3.80 | -2.23 | PF3 | 1716.0 |
| F836 | 778.0 | 3.78 | -1.31 | PF3 | 1718.0 |
| F836 | 780.0 | 3.91 | 1.83 | PF3 | 1720.0 |
| F836 | 782.0 | 3.75 | -2.94 | PF3 | 1722.0 |
| F836 | 784.0 | 3.96 | -4.03 | PF3 | 1724.0 |
| F836 | 786.0 | 3.78 | -3.79 | PF3 | 1726.0 |
| F836 | 788.0 | 4.21 | -3.58 | PF3 | 1728.0 |
| F836 | 790.0 | 4.12 | -0.39 | PF3 | 1730.0 |
| F836 | 794.0 | 4.11 | -1.92 | PF3 | 1734.0 |
| F836 | 798.0 | 4.03 | 0.80 | PF3 | 1738.0 |
| F836 | 800.0 | 4.43 | -0.77 | PF3 | 1740.0 |
| F836 | 802.0 | 4.10 | 1.50 | PF3 | 1742.0 |
| F836 | 804.0 | 4.06 | -3.11 | PF3 | 1744.0 |
| F836 | 806.0 | 4.67 | 0.46 | PF3 | 1746.0 |
| F836 | 808.0 | 4.86 | 1.32 | PF3 | 1748.0 |
| F836 | 810.0 | 5.02 | 0.96 | PF3 | 1750.0 |
| F836 | 812.0 | 4.27 | -1.14 | PF3 | 1752.0 |
| F836 | 814.0 | 3.94 | -0.15 | PF3 | 1754.0 |
| F836 | 816.0 | 4.06 | -0.90 | PF3 | 1756.0 |
| F836 | 818.0 | 3.48 | 1.24 | PF3 | 1758.0 |
| F836 | 820.0 | 3.46 | -1.08 | PF3 | 1760.0 |
| F836 | 822.0 | 4.69 | -0.62 | PF3 | 1762.0 |
| F836 | 838.0 | 4.70 | -0.79 | PF3 | 1778.0 |
| F836 | 842.0 | 1.81 | -4.00 | LMH | 1782.0 |
| F836 | 854.0 | 2.69 | -3.65 | LMH | 1794.0 |
| F836 | 880.0 | 2.14 | -4.53 | LMH | 1820.0 |
| F836 | 888.0 | 1.59 | -7.06 | LMH | 1828.0 |
| F836 | 889.0 | 1.27 | -8.38 | LMH | 1829.0 |
| F836 | 890.0 | 1.48 | -9.16 | LMH | 1830.0 |

Table S2. Carbon and oxygen isotope data tables

| F836 | 891.0 | 0.78 | -1.44 | LMH | 1831.0 |
|------|-------|------|-------|-----|--------|
| F836 | 893.0 | -2.02 | -1.24 | LMH | 1833.0 |
| F836 | 894.0 | -2.15 | -2.94 | LMH | 1834.0 |
| F836 | 895.0 | -4.27 | -2.63 | LMH | 1835.0 |
| F836 | 896.0 | -6.15 | -2.19 | LMH | 1836.0 |
| F836 | 897.0 | -1.67 | -4.09 | LMH | 1837.0 |
| F836 | 899.0 | -1.68 | -4.55 | LMH | 1839.0 |
| F836 | 900.0 | 0.03 | -4.37 | LMH | 1840.0 |
| F836 | 901.0 | -0.45 | -4.68 | LMH | 1841.0 |
| F836 | 902.0 | 0.24 | -2.13 | LMH | 1842.0 |
| F836 | 904.0 | 0.27 | -4.94 | LMH | 1844.0 |
| F836 | 905.5 | 0.32 | -3.41 | LMH | 1845.5 |

F837 at: N64°39.757', W140°00.482'

F840 at: N64°42.431', W140°01.312'

Base of F841 at: N64°45.364', W140°06.928'

| section | height (m) | d13C | d18O | unit |
|---------|-----------|------|------|------|
| F841 | 0.3 | 0.58 | -2.22 | PH2 |
| F841 | 0.5 | -3.75 | -13.57 | PH2 |
| F841 | 4.0 | -2.87 | -13.86 | PH2 |
| F841 | 5.0 | 0.04 | -6.53 | PH2 |
| F841 | 6.5 | 0.36 | -5.00 | PH2 |
| F841 | 14.0 | 0.60 | -5.45 | PH2 |
| F841 | 22.0 | 7.31 | -10.05 | PH2 |
| F841 | 24.2 | -0.12 | -6.86 | PH2 |
| F841 | 40.6 | -2.45 | -5.35 | PH3 |
| F841 | 40.8 | -2.46 | -5.30 | PH3 |
| F841 | 41.0 | -2.52 | -5.26 | PH3 |
| F841 | 41.2 | -2.55 | -5.28 | PH3 |
| F841 | 41.4 | -2.32 | -4.73 | PH3 |
| F841 | 41.6 | -2.60 | -5.53 | PH3 |
| F841 | 41.9 | -2.98 | -5.68 | PH3 |
| F841 | 42.2 | -3.21 | -6.29 | PH3 |
| F841 | 42.5 | -3.31 | -6.00 | PH3 |
| F841 | 43.0 | -3.57 | -5.62 | PH3 |

Base of F917 at: N64°42.458', W140°01.217'

Base of 918 at: N64°45.746', W140°06.449'

Base of 936 at: N64°34.417', W136°50.977'

S8 at: N72°11.275', W111°45.549'

Coates Lake Group at Moose Horn at: ~N63°34', W127°02'

| section | height (m) | d13C | d18O | unit |
|---------|-----------|------|------|------|
| P9E | 38.0 | -4.52 | -1.00 | CC |
| P9E | 58.0 | -5.62 | -1.36 | CC |
| P9E | 60.0 | -5.53 | -3.12 | CC |
| P9E | 67.0 | -5.07 | -2.43 | CC |
| P9E | 73.0 | -6.12 | -8.79 | CC |
| P9E | 75.0 | -5.49 | -8.24 | CC |
| P9E | 77.0 | -5.36 | -8.93 | CC |
| P9E | 80.0 | -4.61 | -8.44 | CC |
| P9E | 82.0 | -4.20 | -8.98 | CC |
| P9E | 85.0 | -3.32 | -9.57 | CC |
| P9E | 86.0 | -3.20 | -5.67 | CC |
| P9E | 88.0 | -2.96 | -6.24 | CC |
| P9E | 90.0 | -2.58 | -7.96 | CC |
| P9E | 92.0 | -1.95 | -12.95 | CC |
| P9E | 94.0 | -1.47 | -13.49 | CC |
| P9E | 98.0 | -0.94 | -13.37 | CC |
| P9E | 110.0 | -0.80 | -12.46 | CC |
| P9E | 117.0 | -0.78 | -8.68 | CC |
| P9E | 118.0 | -0.01 | -7.76 | CC |
| P9E | 119.0 | 0.36 | -6.21 | CC |
| P9E | 122.0 | 0.85 | -1.98 | CC |
| P9E | 125.0 | 0.94 | 0.11 | CC |
| P9E | 135.0 | 1.51 | 2.17 | CC |
| P9E | 140.0 | 1.15 | 2.74 | CC |
| P9E | 141.0 | 0.85 | 0.42 | CC |
| P9E | 143.0 | 0.52 | 1.09 | CC |
| P9E | 146.0 | 1.06 | 0.33 | CC |
| P9E | 150.0 | 0.95 | 0.24 | CC |
| P9E | 154.0 | 1.04 | -1.16 | CC |
| P9E | 157.0 | 0.08 | -3.04 | CC |
| P9E | 160.0 | -0.59 | -5.13 | CC |
| P9E | 161.0 | 0.15 | -2.23 | CC |

**References and notes.**

S1.     R. I. Thompson, C. F. Roots, P. S. Mustard, *Geological Survey of Canada, Open File 2849*, (1994).

S2.     G. Abbott, *Exploration and Geological Services Division, Yukon Region, Bulletin 9*, 1 (1997).

S3.     P. S. Mustard, *Geological Society of America Bulletin* **103**, 1346 (1991).

S4.     P. S. Mustard, J. A. Donaldson, *Journal of Sedimentary Petrology* **60**, 525 (1990).

S5.     P. S. Mustard, C. F. Roots, *Geological Survey of Canada Bulletin* **492**, 0 (1997).

S6.     C. F. Roots, Carleton University (1987).

S7.     G. H. Eisbacher, *Geological Survey of Canada Paper 77-35*, 1 (1978).

S8.     F. A. Macdonald, P. A. Cohen, F. O. Dudás, D. P. Schrag, *Geology* **XXX**, XXX (2010).

S9.     G. M. Young, *Geological Society of America Bulletin* **93**, 759 (1982).

S10.    P. F. Hoffman, D. P. Schrag, *Terra Nova* **14**, 129 (2002).

S11.    N. J. Butterfield, *Precambrian Research* **111**, 235 (2001).

S12.    A. N. LeCheminant, L. M. Heaman, *Earth and Planetary Science Letters* **96**, 38 (1989).

S13.    L. M. Heaman, A. N. LeCheminant, R. H. Rainbird, *Earth and Planetary Science Letters* **109**, 117 (1992).

S14.    D. Y. Sumner, S. A. Bowring, *Precambrian Research* **79**, 25 (1996).

S15.    L. C. Kah, A. G. Sherman, G. M. Narbonne, A. H. Knoll, A. J. Kaufman, *Canadian Journal of Earth Sciences* **36**, 313 (1999).

S16.    N. J. Butterfield, R. H. Rainbird, *Geology* **26**, 963 (1998).

S17.    N. J. Butterfield, *Lethaia* **38**, 155 (2005).

S18.    N. J. Butterfield, *Paleobiology* **31**, 165 (2005).

S19.    A. H. Knoll, E. Javaux, D. Hewitt, P. A. Cohen, *Philosophical Transactions of the Royal Society of London B: Biological Sciences* **361**, 1023 (2006).

S20.    D. S. Jones, Ph.D. thesis, Harvard University (2009).

S21.    A. C. Maloof, G. P. Halverson, J. L. Kirschvink, P. F. Hoffman, D. P. Schrag, *Geological Society of America Bulletin* **118**, 1099 (2004).

S22.    N. J. Butterfield, *Paleobiology* **30**, 231 (2004).

S23.    G. P. Halverson, A. C. Maloof, D. P. Schrag, F. O. Dudas, M. T. Hurtgen, *Chemical Geology* **237**, 5 (2007).

S24.    S. Porter, R. Meisterfeld, A. H. Knoll, *Journal of Paleontology* **77**, 409 (2003).

S25.    K. E. Karlstrom *et al.*, *Geology* **28**, 619 (2000).

S26.    C. M. Dehler *et al.*, *Geological Society of America Bulletin* **117**, 32 (2005).

S27.    M. J. Timmons, K. E. Karlstrom, C. M. Dehler, J. W. Geissman, M. T. Heizler, *Geological Society of America Bulletin* **113**, 163 (2001).

S28.    F. A. Corsetti, A. N. Olcott, C. Bakermans, *Palaeogeography Palaeoclimatology Palaeoecology* **232**, 114 (2006).

S29.    F. A. Corsetti, S. M. Awramik, D. Pierce, *Proceedings of the National Academy of Sciences* **100**, 4399 (2003).

S30.    J. D. Walker, D. W. Klepacki, B. C. Burchfield, *Geology* **14**, 15 (1986).

S31.    G. R. Licari, *Journal of Paleontology* **52**, 767 (1978).

S32.    S. A. Bowring, J. P. Grotzinger, D. J. Condon, J. Ramezani, M. Newall, *American Journal of Science* **307**, 1097 (2007).

S33.    C. Zhou *et al.*, *Geology* **32**, 437 (2004).

S34.    G. P. Halverson, P. F. Hoffman, D. P. Schrag, A. C. Maloof, A. H. N. Rice, *Geological Society of America Bulletin* **117**, 1181 (2005).

S35.    K. H. Hoffmann, D. J. Condon, S. A. Bowring, J. L. Crowley, *Geology* **32**, 817 (2004).

S36.    F. A. Macdonald, D. S. Jones, D. P. Schrag, *Geology* **37**, 123 (2009).

S37.    D. J. Condon *et al.*, *Science* **308**, 95 (2005).

S38.    G. D. Love *et al.*, *Nature* **457**, 718 (2009).

S39.    L. Yin *et al.*, *Nature* **446**, 661 (2007).

S40.    P. A. Cohen, A. H. Knoll, R. B. Kodner, *Proceedings of the National Academy of Sciences*,  (2009).

S41.    S. Xiao, A. H. Knoll, X. Yuan, C. M. Pueschel, *American Journal of Botany* **91**, 214 (2004).

S42.    P. F. Hoffman, Z.-X. Li, *Palaeogeography Palaeoclimatology Palaeoecology* **277**, 158 (2009).

S43.    S. A. Bowring, P. M. Myrow, E. Landing, J. Ramezani, *Geophysical Research Abstracts* **5**, 219 (2003).

S44.    J. M. Mattinson, *Chemical Geology* **220**, 47 (2005).

S45.    T. E. Krogh, *Geochimica et Cosmochimica Acta* **37**, 485 (1973).

S46.    H. Gerstenberger, G. Haase, *Chemical Geology* **136**, 309 (1997).

S47.    M. D. Schmitz, B. Schoene, *Geochemistry, Geophysics, Geosystems - $G^3$* **8**, no. 8 (2007).

S48. D. Condon *et al.*, *Eos, Transactions, American Geophysical Union* **88**, Abstract V41E (2007).

S49. A. H. Jaffey, K. F. Flynn, L. E. Glendenin, W. C. Bentley, A. M. Essling, *Physical Review C* **4**, 1889 (1971).

S50. C. F. Roots, R. R. Parrish, *Radiogenic age and isotopic studies, Geological Survey of Canada, Paper 88-2*, 29 (1988).

S51. B. Schoene, J. C. Crowley, D. J. Condon, M. D. Schmitz, S. A. Bowring, *Geochimica et Cosmochimica Acta* **70**, 426 (2006).

S52. R. H. Rainbird, C. W. Jefferson, G. M. Young, *Geological Society of America Bulletin* **108**, 454 (1996).